VYSOKÉ UČENÍ TECHNICKÉ V BRNĚ
BRNO UNIVERSITY OF TECHNOLOGY

FAKULTA STROJNÍHO INŽENÝRSTVÍ
ENERGETICKÝ ÚSTAV

FACULTY OF MECHANICAL ENGINEERING
ENERGY INSTITUTE

INFLUENCE OF OPERATIONAL CONDITIONS ON SPRAY CHARACTERISTIC OF TWIN-FLUID ATOMIZERS

VLIV PROVOZNÍCH PARAMETRŮ NA KVALITU ROZPRAŠOVÁNÍ U DVOU-MÉDIOVÝCH TRYSEK

DIPLOMOVÁ PRÁCE
MASTER´S THESIS

AUTOR PRÁCE — Bc. MATOUŠ ZAREMBA
AUTHOR

VEDOUCÍ PRÁCE — Ing. JAN JEDELSKÝ, Ph.D.
SUPERVISOR

BRNO 2013

Vysoké učení technické v Brně, Fakulta strojního inženýrství

Energetický ústav
Akademický rok: 2012/2013

ZADÁNÍ DIPLOMOVÉ PRÁCE

student(ka): Bc. Matouš Zaremba

který/která studuje v **magisterském navazujícím studijním programu**

obor: **Fluidní inženýrství (2301T036)**

Ředitel ústavu Vám v souladu se zákonem č.111/1998 o vysokých školách a se Studijním a zkušebním řádem VUT v Brně určuje následující téma diplomové práce:

Vliv provozních parametrů na kvalitu rozprašování kapalin u dvou-médiových trysek

v anglickém jazyce:

Influence of operational conditions on spray characteristics of twin-fluid atomizers

Stručná charakteristika problematiky úkolu:

Dvoumédiové trysky, tedy trysky, které pro rozprašování kapalin používají pomocný plyn, jsou v současnosti oblíbené v aplikacích, kde je důležité zajistit jemný sprej při nízkém atomizačním tlaku. Struktura a geometrie spreje, velikost a rychlost generovaných kapek patří mezi důležité a sledované parametry trysek pro atomizaci kapalin. Tyto vlastnosti budou na konkrétní trysce zkoumány pomocí optických měřících metod.

Cíle diplomové práce:

- Úprava zkušebního zařízení pro provoz dvou-médiových trysek
- Příprava a nastavení optického měřícího systému
- Měření vybraných vlastností spreje
- Analýza výsledků, popis spreje a vyhodnocení vlivu provozních podmínek. Grafická prezentace výsledků.
- Výrobní dokumentace trysek

Seznam odborné literatury:

[1] Bayel, L., Orzechowski, Z., Liguid atomization, Taylor & Francis, Washington, D.C., 1993
[2] Lefebvre, A.H., Atomization and Sprays, Hemisphere, Washington, D.C., 1989
[3] M. Pavelek, E. Janotková, J. Štětina: Vizualizační a optické měřicí metody, Accessed via WWW, URL: http://dt.fme.vutbr.cz/~pavelek/optika/, (31 Oct. 2006).
[4] ZHANG, Zh., LDA Application Methods: Laser Doppler Anemometry for Fluid Dynamics (Experimental Fluid Mechanics), Springer, ISBN: 9783642135132, 2010.
[5] Lehner, M.; et al.: Applied Optical Measurements: Heat and Mass Transfer, ISBN 3 540 66173 5 (hbk), (Berlin: Springer) 462 pp, 1999
[6] Dantec, TSI - firemní literatura

Vedoucí diplomové práce: Ing. Jan Jedelský, Ph.D.

Termín odevzdání diplomové práce je stanoven časovým plánem akademického roku 2012/2013.

V Brně, dne 20.11.2012

L.S.

doc. Ing. Zdeněk Skála, CSc.	prof. RNDr. Miroslav Doupovec, CSc., dr. h. c.
Ředitel ústavu	Děkan fakulty

Summary:

This master's thesis deals with measurement of spray characteristics of Effervescent atomizers intended for burning waste and heavy fuels. Atomizers were tested on cold test bench by means of Phase Doppler Anemometry. Spray characteristics were evaluated for many different regimes of pressure, temperature and Gas to liquid ratio. The aim of this measurement is to compare flow regimes and their influence on the quality of spray characteristics.
The theoretical part describes basic fundamental principles of liquid atomization, effervescent atomization and principles of laser diagnostic methods. The practical part is engaged with improvements in test bench and setting up and optimization of the laser measuring system. Results contain visualization of spray, velocity profiles and drop size distribution in various operating flow regimes of the jet.

Key words:

Atomization, spray, droplet, measuring volume, effervescent atomizer, Laser Doppler Anemometry, LDA, Phase-Doppler Anemometry, PDA

Abstrakt:

Tato diplomová práce se zabývá měřením charakteristik sprejů šumivých trysek určené pro spalování odpadních a těžkých paliv. Trysky byly testovány za studena pomocí fázové Dopplerovského analyzátoru. Charakteristiky sprejů byly vyhodnoceny z vice různých provozních režimů tlaku, teploty a poměru plynu a kapaliny. Cílem těchto měření je porovnat provozní režimy a jejich vliv na kvalitu spreje.
Teoretická část se zabývá základy rozpadu kapalin, rozpad v šumivých tryskách a principy laserových měřících metod. Praktická část se zabývá úpravou testovací tratě, nastavení a optimalizací měřícího laserového zařízení. Výsledky obsahují vizualizaci spreje, rychlostní profily a distribuci velikosti kapek při různých provozních režimech trysky.

Klíčová slova:

Atomizace, sprej, kapka, měřící objem, šumivá tryska, laserová dopplerovská anemometrie, LDA, lázový doplerovský analyzátor, PDA

Bibliografic citation:

ZAREMBA, M. *Influence of operation conditions on spray characteristics of twin fluid atomizers.* Brno: Vysoké ucení technické v Brne, Fakulta strojního inženýrství, 2012. 81 s. Vedoucí diplomové práce Ing. Jan Jedelský, Ph.D.

VUT-EU-ODDI-13303-13-13

Affirmation:

I declare that this master's thesis is the result of my own work led by Ing. Jan Jedelský, Ph.D. and all used sources are duly listed in the bibliography.

Bc. Matouš Zaremba

VUT-EU-ODDI-13303-13-13

Preface

The phenomena of liquid atomization has become important in many applications. Quality of atomization has crucial effect on combustion processes such as gas turbines, diesel engines, rockets and also in industry processes like spray drying, evaporation cooling, spray painting. They are also important for other applications in medicine or meteorology. The most used atomizing liquid is water or hydrocarbon fuels. Due to different requirements for each application various designs of atomizers were developed.

During time scientists have found ways how to examine spray structure without disturbing flow structure. The most used methods usually employs lasers to examine velocity distribution, droplets size, cone angle, mass distribution etc. which are of interest in most applications. The most common methods are LDA, PDA, PIV, LIF.

This thesis is focused on setting up a measuring system and measuring characteristic of Effervescent jet in different flow regimes. The examined jet was designed within this thesis. For measurements Phase Doppler Analyzer was used. This method is focused on droplet size and velocity measurements.

The thesis is divided into 8 chapters. In the first chapter is described partition of common used atomizers. The second chapter describes basic principles of liquid atomization and atomization in Effervescent nozzles. Chapter 3 deals with design of tested nozzle. In chapter 4 the reader can find principles of laser diagnostic techniques used for measurements. Chapter 5 covers the improvements of the test bench. Chapter 6 focuses on the experimental setup which describes the setup procedure. Results of experiments are summarized in Chapter 7 and Chapter 8 concludes this thesis.

In appendices drawings are attached. They were made for manufacturing the examined jet. Supporting graphical material can be found on attached DVD.

Acknowledgments:

I would like to express my gratitude to my supervisor Ing. Jan Jedelský Ph.D. for his guidance and patience during the whole project. I appreciate his willingness to discuss many different topics and help me with problems I was facing.
I am also thankful that I had the opportunity to work with equipment which was purchased under the project NETME Centre reg No.: CZ 1.05/2.1.00/01.0002, id. Code ED0002/01/01, financed from Operational Programme Research and Development for Innovation, which is co-funded by ERDF (European Regional Development Fund).

I would like to express my thanks to students Adam Bolcek and Milan Malý who helped me with high frequency camera setup and preparations. They were very willing to help me even under time pressure.

I must also acknowledge skills of Roman Partika who made every part I had designed. I am also thankful for his advice on manufacturing each part which was made.

I would also like to thank my family for the support they have provided me through my entire life. They have encouraged me at every moment I have spent at the university. Without them, it would be impossible to accomplish my study successfully.

CONTENTS

BRNO UNIVERSITY OF TECHNOLOGY 1
Summary: 3
Key words: 3
Abstrakt: 3
Klíčová slova: 3
Bibliografic citation: 5
Affirmation 7
Preface 9
Acknowledgments: 11
Contents 13
1. Classification of atomizers 17
1.1 Pressure atomizers 17
1.2 Rotary atomizers 18
1.3 Air-assist atomizers 18
1.4 Effervescent atomizers 19
1.5 Air-blast atomizers 20
2. Atomization in effervescent sprays 21
2.1 Principles of liquid atomization 21
2.2 Disintegration of the droplet 23
2.3 Effervescent atomization 25
3.1 Nozzle discharge parameters 30
3.2 Drop-size distributions of sprays 34
3.3 Droplet size 36
3. Design of the tested nozzle 39
4. Laser anemometry 43
4.1 LDA characteristics 43
4.2 Doppler effect 44
4.3 Frequency shift 46
4.4 Lorenz-Mie light scattering theory 47
4.5 Backscatter versus forward scatter LDA 48
4.6 Phase Doppler Anemometry 50

5. Test bench 57
5.1 Fuel supply system 57
5.2 Pressured air supply system 58
5.3 3D traverse system 59
6. Experimental setup 61
6.1 PDA measuring system 61
6.2 Description of setting up the PDA system 62
6.3 Atomizing liquid 69
7. Results 71
7.1 Visualization of spray 71
7.1 Cone angle 75
7.2 Axial velocity profiles comparison 77
7.3 Radial velocity profiles comparison 80
7.4 Drop size distribution 82
7.5 Measurement uncertainty 86
8. Conclusion 87
8.1 Goals 87
8.2 Spray characteristics 87
Bibliography 89
List of symbols 91

1. CLASSIFICATION OF ATOMIZERS

[1], [2], [3], [4]

Atomization is a process of breaking up liquid into smaller droplets in gaseous atmosphere. It is of importance in many industrial, agricultural, medical and meteorology applications. It has crucial effect on combustion processes where larger liquid surface area leads to finer combustion process and lower exhaust emissions. The atomizers are components, which force liquids to break up. Every application requires a different type of spray, that is why many different atomizers have been developed.
Atomization is usually achieved by discharging the liquid at high velocity into a relatively slowly moving stream of air or gas. Another way, how to accomplish atomization is to expose slowly moving liquid to a high velocity stream of gas. Other method of atomization is to use additional medium such as air into the jet and bubbles of air spread rapidly when they pass through orifice exit of the atomizer and helps the liquid to be atomized.
The most commonly used atomizers are described below.

1.1 Pressure atomizers

Pressure atomizers are based on the principle of transferring pressure energy into kinetic energy to achieve high velocity between the liquid and the ambient gas. These atomizers are the most common types of atomizing devices. Their main advantages are simple construction, no additional energy input and no additional medium requirements. Due to these characteristics, the pressure atomizers are the most used in industrial applications. They include more solutions of construction. The constructional simplest atomizers are called plain-orifice nozzle **Figure 1-1**. The simple circular orifice of the atomizer produces the narrow spray cone angles of about 10°. Usually this is not the required shape of the spray, that is why it a trend to extend angles to 30° – 150°. These angles can be achieved by pressure-swirl atomizers. Swirling motion is achieved by rotary speed component of fluid. When liquid emerges from the discharge orifice, it spreads more radially than circular simple orifice nozzle.
Pressure atomizers are limited by relationship between liquid flow rate and given pressure. That is why atomizers have restricted operational range of liquid flow.
The need to handle wide range of flow rates led to development of dual-orifice nozzle **Figure 1-1**. This type was widely used in aircraft and industrial gas turbines. It is consist of two simplex nozzles which are fitted concentrically one inside. In case of low flow rates, liquid passes through the primary nozzle. When flow rate exceeds certain value as well as the pressure the pressurizing valve opens and puts into operation the secondary nozzle.

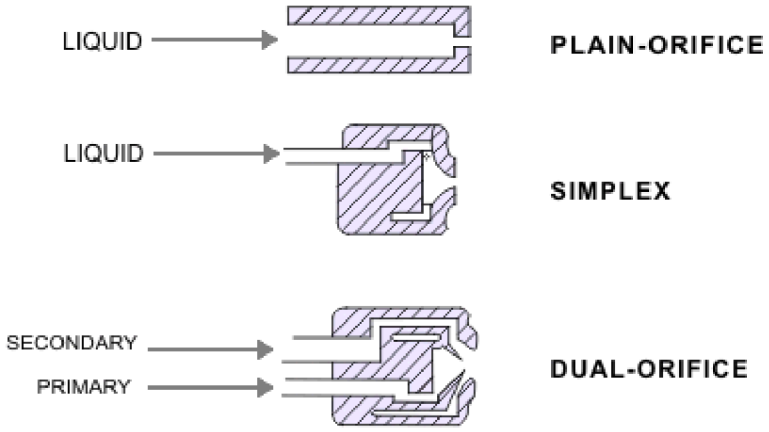

Figure 1-1 Pressure nozzles. [4]

1.2 Rotary atomizers

Rotary atomizers are based on principle of the centrifugal force. The liquid falls on the rotating surface and then it flows radially to the edge of the rotating surface. Here liquid spreads out into the ligaments and breaks up into fine drops of fairly uniform size. They are insensitive to the viscosity and contaminants in the atomizing liquid. Disadvantage of this type of atomizer is input power requirements.

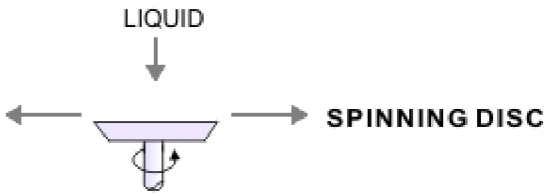

Figure 1-2 Rotary atomizer. [4]

1.3 Air-assist atomizers

Air-assist atomizers also known as Twin fluid atomizers employ the kinetic energy of the air stream to disintegrate liquid jet or sheet into ligaments and then drops. Air-assist atomizers replace simplex nozzles at low fuel flows and provide much better atomization due to high velocity air stream. This enables us to operate with low flow rates and low pressures. Two types of air-assist atomizers have been developed. Atomizers with internal and external mixing, see following figure:

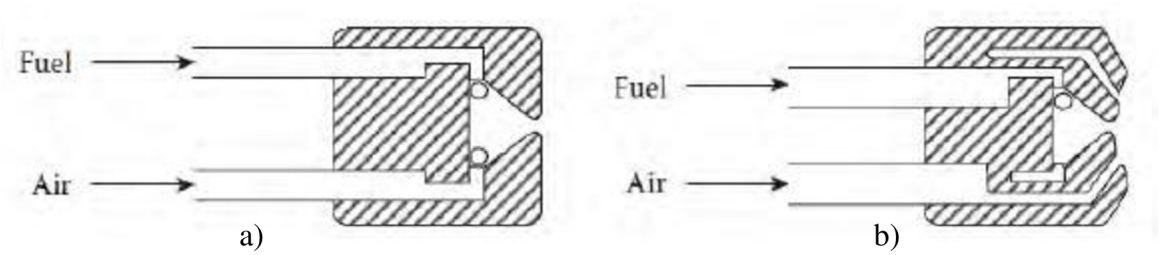

Figure 1-3 Construction of air-assist atomizers: a) internal mixing b) external mixing. [1]

The main drawback of this type of atomizer is the need of external supply of high-pressure air. This is the reason why they cannot be used in aircraft applications and determines them to larger use in big industrial engines.

1.4 Effervescent atomizers

The main difference between the previous atomizers and effervescent is that air is injected into the nozzle at some point upstream of the discharge orifice. This concept involves a plain-orifice atomizer with means of injecting air (or gas). Air is injected at low velocity and its function is not to impart kinetic energy but only to create bubbles in flow. The pressure difference between gas and liquid is small. The gas has to overcome the resistance needed to enter into the flowing liquid. The main advantages of effervescent atomizers are:

1. Good atomization at very low injection pressure and low gas flow rates.
2. Effervescent jets eliminate problems with plugging because of their larger orifice diameters.
3. The aeration of the spray improves combustion processes such as alleviating soot formation and exhaust smoke.
4. Simple construction and large orifice diameters leads to good reliability, easy maintenance and low costs.
5. In comparison to the other twin-fluid atomizer, less amount of air is needed to provide fine atomization.
6. Mean drop size is relatively insensitive to liquid viscosity.

The main drawback of the effervescent atomizers is pressured air requirements, which must be provided essentially at the same pressure as that of the liquid. Another disadvantage is that this type of atomizer produces wide distribution of droplets (correspond to q of around 2 in Rosin-Rammler distribution, it will be described in the next chapter)

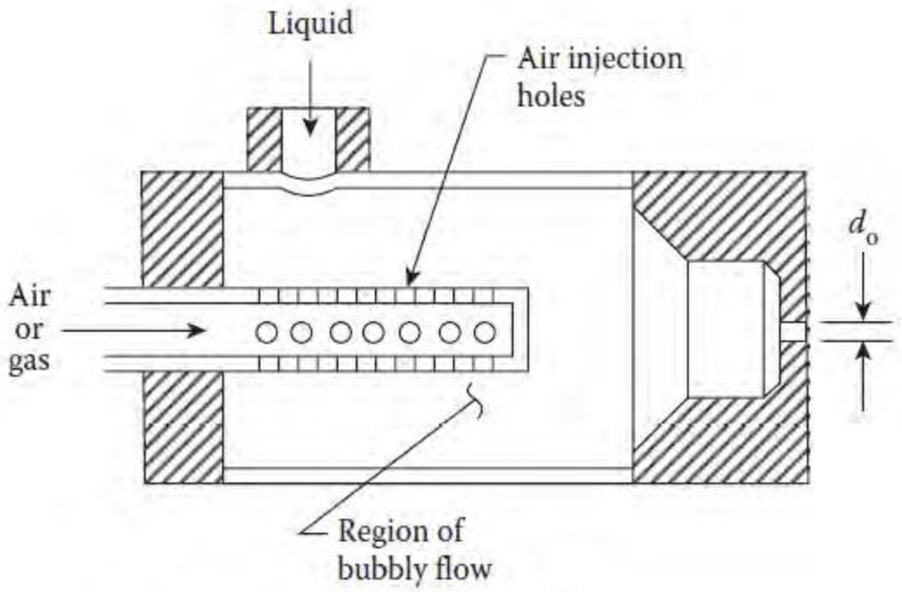

Figure 1-4 Schematic layout of effervescent atomizer. [1]

1.5 Air-blast atomizers

The principle of the air-blast atomizers is very similar to the air-assist atomizers. The additional air causes liquid breakup into ligaments and then into drops. The main difference between those two types is the quantity of air employed and its atomizing velocity. The air-assist atomizers operate in relatively small ranges of very high velocity air. Unlike air-blast atomizers which are limited by maximum velocity of the air (around 120 m/s) a larger amount of air is needed to provide good atomization. Due to quantity of the added air, better combustion process is achieved (low soot formation, low flame radiation and minimum of exhaust smoke).

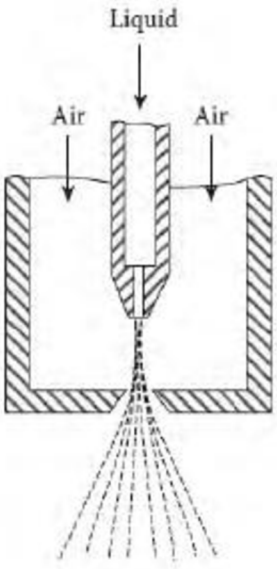

Figure 1-5 Air-blast atomizer. [4]

2. ATOMIZATION IN EFFERVESCENT SPRAYS

[1], [2], [3], [5], [6]

2.1 Principles of liquid atomization

Atomization is a process of breaking up liquid into smaller droplets in gaseous atmosphere. For description of atomization process we can divide atomization into two areas. *Primary atomization* is located near the orifice of the atomizer where liquid stream is disintegrated into ligaments due to cohesive and disruptive forces, which gives rise to oscillations and perturbations. This process is dependent on internal design of atomizer and properties of ambient air.
The other area called *Secondary atomization*, where large drops which exceed critical size, are further disintegrated into smaller droplets. Breakup of large droplets is influenced by movements and interactions between droplets in ambient air. Secondary atomization is located further downstream from the nozzle.
These properties determine spray characteristics such as drop size, droplet velocity and spray angle. Other major characteristic that affects spray parameters are liquid density, surface tension and viscosity.

Liquid density can be determined as mass per unit volume of the liquid *L* under certain conditions (pressure, temperature):

$$\rho_L = \frac{m_L}{V_L}. \tag{1.1}$$

Temperature usually influences liquid density. The following equation gives us relation between liquid density and its temperature:

$$\rho_{L,2} = \frac{\rho_{L,2}}{1+\alpha\Delta T}, \tag{1.2}$$

Where α is mean volumetric expansion coefficient in the given ΔT and $\rho_{L,1.2}$ is liquid density in states 1 and 2. The influence of liquid density on atomization processes is negligible due to small differences in typical operation conditions using commonly atomized liquids such as water or hydrocarbon fuels.
Commonly used liquid has low compressibility that is why the influence of pressure on liquid density will also be neglected. Exceptions are applications where pressure operating range is in order of tens of MPa.

Viscosity can be described as a level of fluidity or as a measure of the resistance of fluid in motion against the acting stresses. The relationship between shear stress τ, dynamic viscosity μ and velocity gradient *dv/dy* can be written as:

$$\tau = \mu \frac{dv}{dy}, \tag{1.3}$$

commonly known as Newton's law of viscosity which is derived for laminar flow. From dynamic viscosity and liquid density, kinematic viscosity ν can be calculated:

$$\nu = \frac{\mu}{\rho}. \tag{1.4}$$

Viscosity has generally significant effect on atomization of liquids. According to Bayvel and Orzechowski [7] for low viscose liquids, viscosity has only low influence on atomization. But considering dependency on temperature, fuels are usually highly dependent. In many applications it is necessary to preheat fuel before atomization process to decrease viscosity and achieve better atomizing characteristics. Other way to improve atomization of highly viscose fuels is to use air assist atomizers.

Surface tension is not a property of liquid but it is a characteristic of interface between two phases or two separated liquids. It can be defined as contractive tendency of the surface of a liquid that allows it to resist an external force. It can be expressed as the ratio of the surface energy (so-called Gibson free energy) dE to the increase of the liquid surface dA:

$$\sigma = \frac{dE}{dA}. \tag{1.5}$$

The SI unit for this property is $N.m^{-1}$ or commonly used unit $J.m^{-2}$. Early findings by Bayvel and Orzechowski [7] have related that surface tension has no demonstrable effect on the size spectrum for high discharge velocities. On the other hand, newer findings by Liu [8] revealed that an increase in surface tension increases the mean droplet size but only for pressure-swirl atomization. For low viscid liquids Lefebre and Ballal [1] have emphasized the importance of the Weber number as dimensionless value which gives us the relationship between aerodynamic forces and surface tension and therefore it is parameter for correlating drop-size data. Only exception is in case of high Weber numbers where aerodynamic forces have significant influence on the interaction between gas and liquid. Weber number can be calculated from the following equation:

$$We = \rho_A U_R^2 D/\sigma, \tag{1.6}$$

where $U_R$is the relative gas/liquid velocity and σ/D is surface tension force.

Nowadays it is customary to explain liquid breakup on the principle of the liquid sheet or jet breakup in low velocities and pressures of the fluid. In the range of high velocities and pressures liquid sheets or jets do not have time to develop and are immediately disintegrated. This phenomena is known as prompt atomization. For detailed description of atomization reader is referred to Lefebvre [2] or Lin [9].

2.2 Disintegration of the droplet

As already mentioned above the Secondary atomization is a process where droplets from the detachment from the liquid sheets or jet may split into smaller droplets due to interaction between the droplets and ambient air.

The surface area of the liquid sheets or jet increases until it becomes unstable and is disintegrated into drops. Aerodynamic forces are considered as a dominant influence of disintegration in laminar flows. In case of highly developed turbulent flow it can break up without the application of external aerodynamic forces. Even when liquid is injected into vacuum, the jet will disintegrate solely under influence of its own turbulence.

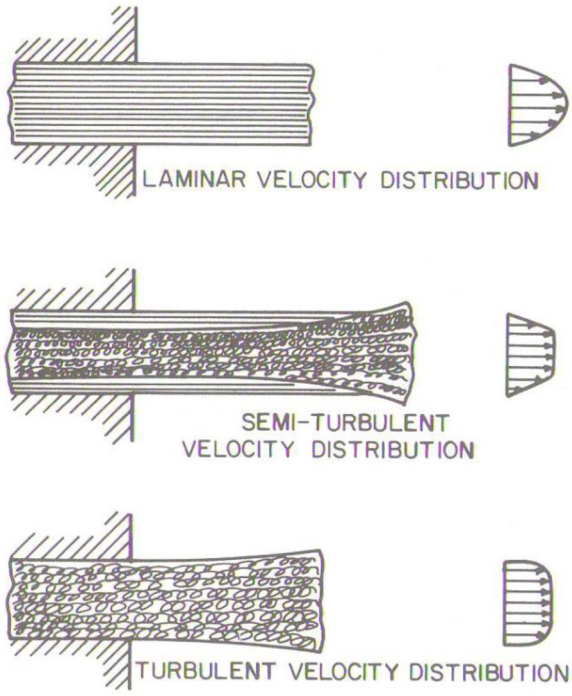

Figure 2-1 Different velocity profiles in laminar, semi-turbulent and turbulent states. [2]

This characteristic behavior is important in many applications such as aerodynamics and propulsion (e.g. mixing and combustion of fuel droplets).

Many different experimental studies have been used to improve description of the breakup of drops. Most of them performed their experiments on Newtonian fluids such as

water, hydrocarbon fuels and so on. The following description is deduced under condition of Newtonian liquids only.

The mode of the drop disintegration depends on whether the drop is subjected to steady acceleration or is suddenly exposed to a high-velocity gas stream. In case of steady acceleration the drop becomes increasingly flattened and at a critical relative velocity it is blown out into the form of a hollow bag attached to a roughly circular rim, see **Figure 2-2**. From this point disintegration produces two types of drops. The first produces a shower of small drops and the second one (the rim) breaks up into large drops. 70% of the mass is concentrated in the rim. This is also known as the *Bag breakup*. It is characteristic for low Weber numbers between 12 and 50. For even lower Weber numbers *Vibrational breakup* is described. It is the case where oscillation leads to breakup into few large fragments.

In many cases it is necessary to produce the smallest possible droplet size while at the condition of the lowest energy inputs. The bag model of breakup is usually the most convenient way to produce fine distribution of drops. The advantage of the bag breakup is low energy input needed to achieve Secondary atomization.

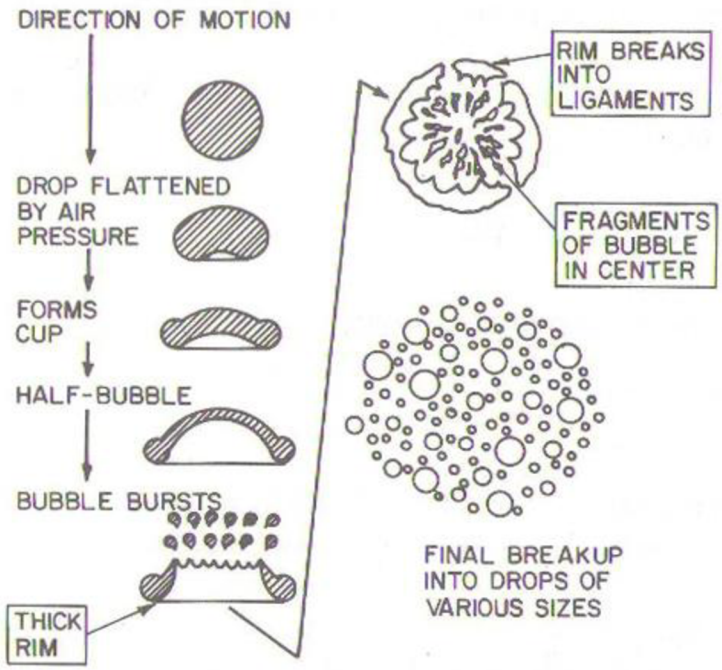

Figure 2-2 Bag breakup. [2]

2.3 Effervescent atomization

[5], [6]

The effervescent atomizers were developed by Lefebvere and his colleagues (Wang and Martin) in the late 1980s, though there are works that mention comparable constructions prior to Lefebvere (Chawla 1985). Over time it has become more and more commonplace in many engineering applications.
Taking into account the previous chapter we can estimate that the effervescent atomizers are used for applications in a wide range of operational conditions and even for low-grade fuels. They are suitable for residual fuels, slurry fuels or waste oil combustion.

The effervescent atomizers fall into the category of "internal mixing". Three different examples of the internal construction are shown in the following figure:

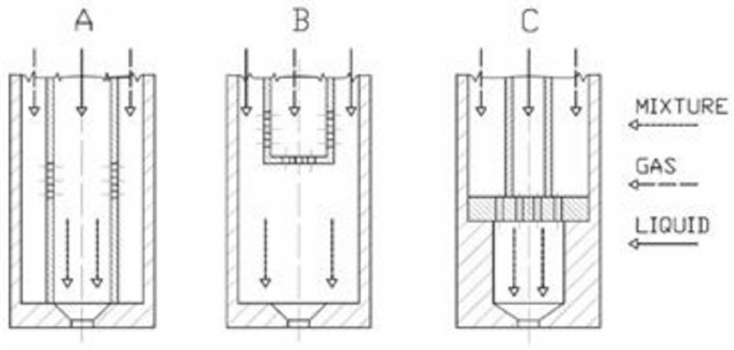

Figure 2-3 Different constructions of effervescent atomizers. [6]

The simple effervescent atomizer consists of four main components: liquid and gas supply inputs, a mixing chamber and exit orifice. Standard proportions of the atomizer are around 100 mm in length, mixing chamber about 5-25 mm long and exit orifices lying between 0.1 and 2.5 mm.
The effervescent atomizers overcome single-fluid techniques because of the difference between velocities of sound in different fluids. The mixture of air and liquid has rapidly lower velocity of sound (20-30 m/s) than velocity of sound in the individual phases (air 300 m/s and water 1500 m/s at standard physical conditions: temperature and pressure). Two-phase flow is choked at a significantly lower velocity in nozzle than that at which a single-phase flow would choke. Thus a two-phase flow will have a steep pressure jump at the nozzle exit at relatively lower velocities and pressures than single-phase flow. Atomization is controlled by the sudden pressure drop that is why it is possible to achieve a good atomization at low injection pressures. Moreover, two-phase flow can remain choked while flowing through orifices larger than those required for single-phase flows. That leads to better atomization even with larger exit orifices.

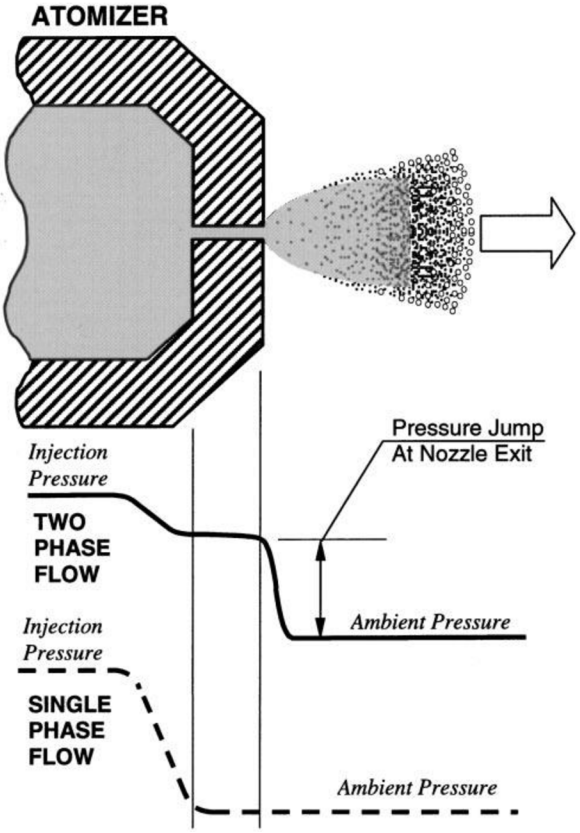

Figure 2-4 Comparison between two-phase flow and single-phase flow at low injection pressure. [5]

The experimental studies were provided by Lefebvere and Sojka and their coworkers. They observed (as we can see in **Figure 2-5**) that three flow regimes exist in effervescent jets.

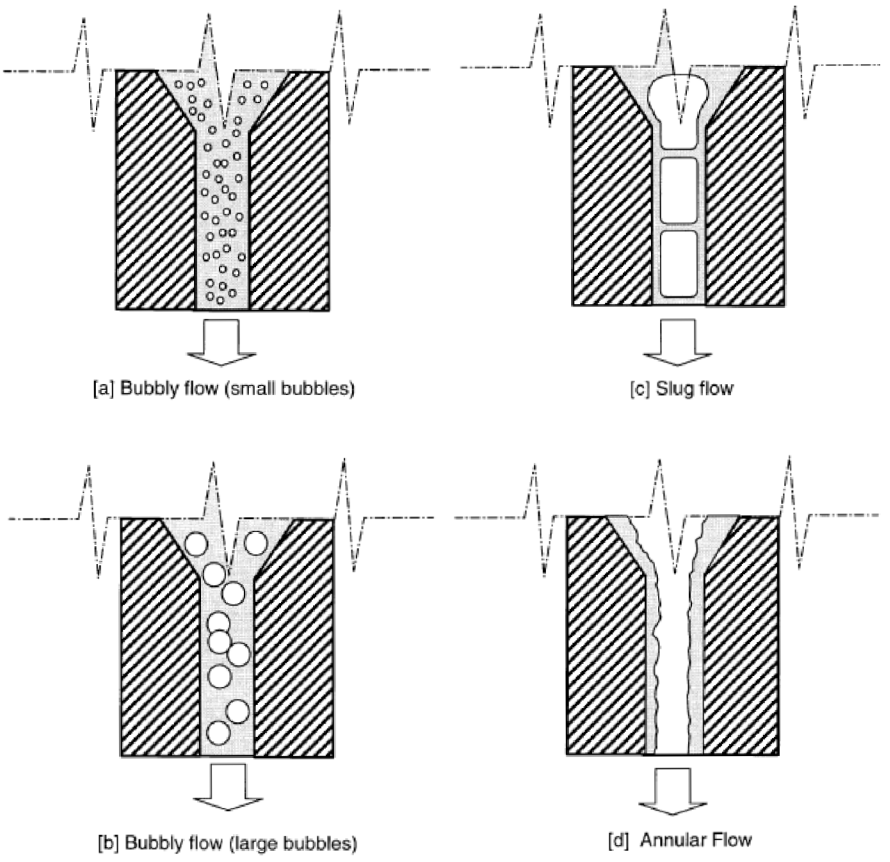

Figure 2-5 Different flow regimes in the discharge orifice. [5]

Bubbly flow is formed in the mixing chamber and it flows towards the nozzle. When this flow exceeds orifice due to the pressure relaxation it expands rapidly and shatters the liquid into drops as shown schematically in **Figure 2-6**.

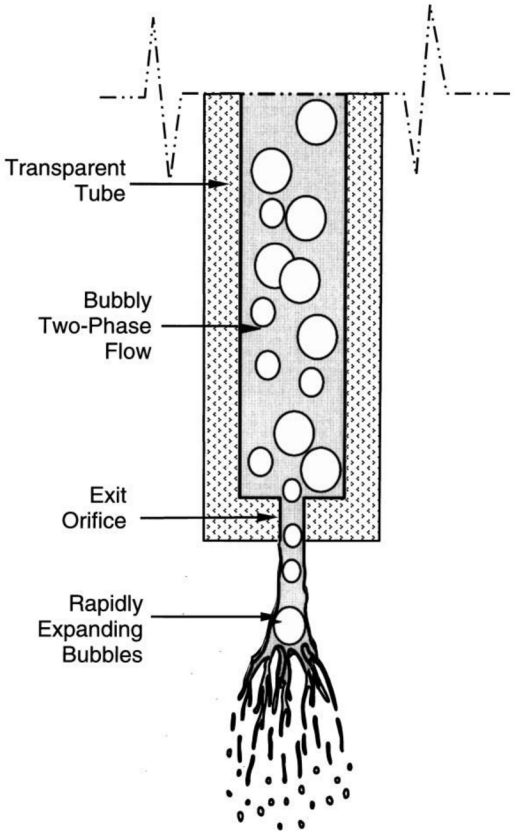

Figure 2-6 Schematic description of the mechanism observed by Roesler and Lefebvre. [5]

Liquid is "squeezed" by the gas bubbles into thin shreds or ligaments. This phenomenon has crucial effect on drop size distribution because it is well established that pressure or air-blast atomization are roughly proportional to the square root of the initial thickness of the ligaments. That is why the increase in amount of air leads to smaller droplets, which are created by explosions of bubbles after they pass through the exit orifice. The diameter of each ligament (and subsequently droplets) is considerably smaller than diameter of the orifice. Thus even in this flow regime, effervescent atomizers are able to produce fine spray. Bubbly flow is generally produced by a maximum value of GLR (gas to liquid ratio) around 5%. In this regime is relatively constant mean drop size within the radial profile comparing the other regimes. In higher ranges of GLR *Slug flow* is formed (**Figure 2-5** [c]).

In Slug flow the atomization principle is very similar to process with Bubbly flow. This is the key feature of effervescent atomization. In Slug flow regime the pressured air expands in similar way as in the Bubbly flow and it has similar effect on liquid atomization.

The third regime of the effervescent atomizers is *Annular flow* (see **Figure 2-5** [d]). Liquid is formed into annular sheet and then it is shattered into thin ligaments. Under the action of aerodynamic forces ligaments break up into fragments and then they are

stabilized into drops (**Figure 2-6** and **Figure 2-7**). This type of flow is characteristic in flow with higher range of GLR.

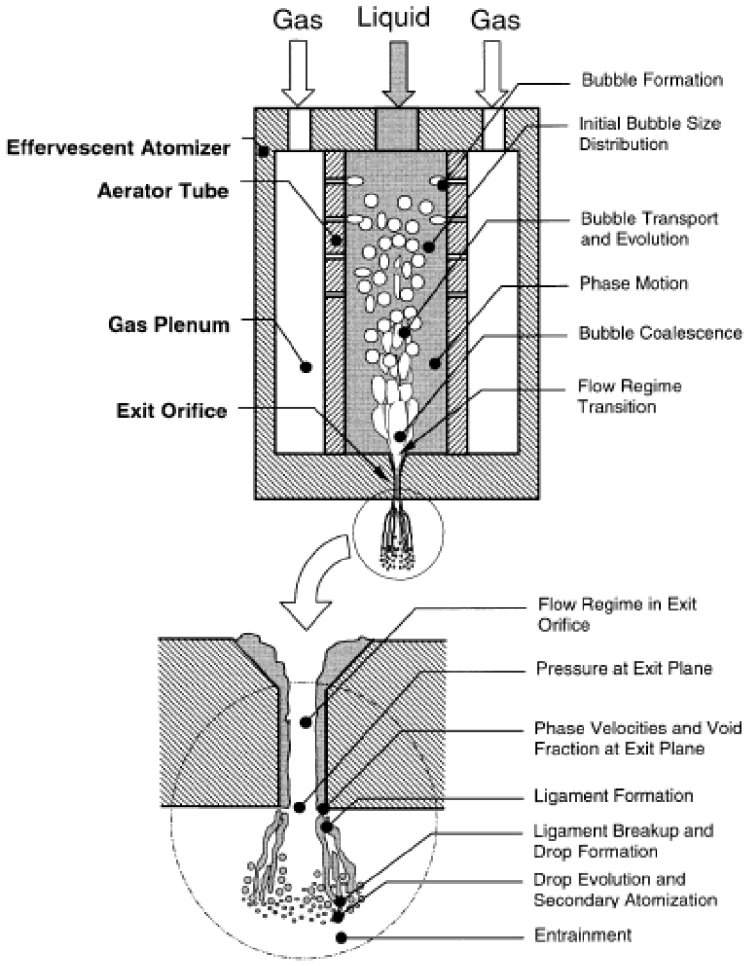

Figure 2-7 Atomization in *Annular flow*. [5]

In Slug and Annular regimes mixture is less homogenous that in bubbly regime. Air occupies mainly center of the final orifice and liquid is attached to the walls of the atomizer due to adhesive forces. The pressure energy of air is concentrated in the center of the final orifice and provides good atomization along the atomizers axis. Due to this behavior at the borders of the spray large droplets are concentrated.

Generally atomizing gas in effervescent jets has two separate functions:

1. The gas inside atomizer reduces the size of the liquid shreds and ligaments which are then disintegrated into drops.
2. The exploding gas has shattering effect on the liquid leaving the nozzle.

A large number of different internal constructions were developed for many applications. The popularity of the twin fluid atomizers has increased in the past few decades. Mostly for their ability to produce fine spray at low pressure even for high-viscosity liquids.

3.1 Nozzle discharge parameters

[5]

For many applications the most important properties are mean drop size, drop size distribution, droplet number density, cone angle and penetration. Usually mean drop size is used to assess the quality of the spray in industrial applications. From the many various definitions of mean drop size, the Sauter mean diameter (SMD or D32) is the most widely used parameter. Mainly in heat and mass transfer applications, such as spray drying and the combustion of liquid fuel sprays.
Although atomization has been studied for more than a hundred years the physical processes in nozzles have not yet been sufficiency well understood. That is why the investigations of the mean drop size distribution has been empirical in nature. However, we have a considerable amount of information from which a number of general conclusions on the effects of internal design and liquids properties on mean drop size can be drawn.

2.5.1. Drop velocity

[5]

Drop velocity is another parameter of interest in spray characteristic. It is important for paint sprays or agricultural applications and others.
The influence of the injection pressure shows similar results as for other conventional atomizers. Drop velocity increases with increasing injection pressure. Another finding indicated the influence of GLR. A bigger amount of atomizing air causes stronger aerodynamic drag forces to drops and causes them to move faster. Panchagnula and Sojka studied the radial and axial drop velocity distribution. Their measurements indicated that the highest velocities are in the center of spray and they falls rapidly in increase of radial direction. Following Figure shows velocity distribution in spray.

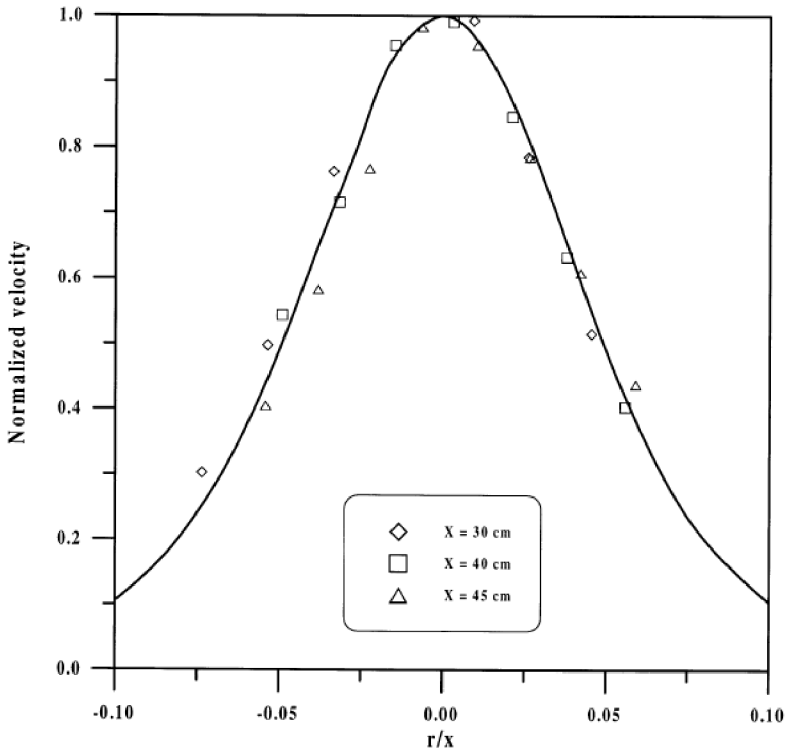

Figure 2-8 Spray velocity distribution in radial direction. [5]

Measurements in axial direction show similar behavior as other twin fluid or pressure atomizers. The drop velocity decreases as distance of measured point is moved downstream.

2.5.2. Parameters affecting drop size

[5], [6]

Drop size distribution is important in many industrial applications. The following paragraphs describe few main parameters which influence mean drop size.

Influence of the initial pressure:

The mean drop size distribution for Newtonian liquids is highly dependent on initial pressure. Generally, it has higher influence in lower injection pressures than in cases of high injection pressures. Following figure shows dependency of the SMD on the initial injecting pressure.

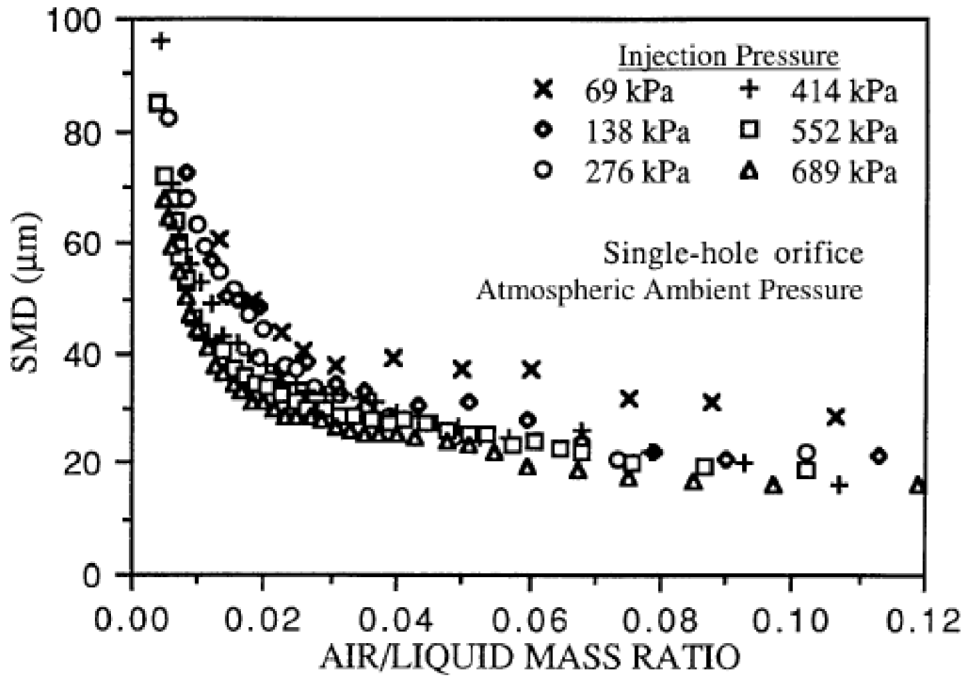

Figure 2-9 Dependency of SMD and injection pressure on GLR. [5]

It was measured on the spray axis 152 mm downstream from the exit orifice at relatively low injection pressures. The range of the pressure is of interest for gas turbines or spray coating applications.
For Non-Newtonian and highly viscous liquids (up to 0.968 kg/ms) it was pointed out that there is no relationship between initial pressure and drop size distribution.

Influence of the GLR ratio:

The GLR value is of importance in most applications of effervescent application. General tendencies are to decrease the amount of atomizing gas to minimum and provide good atomization while maintaining a small mean drop size. Experiments show that relationship between the GLR and mean drop size is a non-linear function where, as GLR is increased, drop size is decreases rapidly (Figure **2-9**). This conclusion was obtained by Roesler and Lefebvere for the range of GLR from 1 to 8,5% which is the range of most effervescent atomizers.

Influence of liquid type:

Newtonian fluids are used for most industrial applications. Non-Newtonian fluids were examined by Sojka and Buckner. They pointed out that spray SMD for non-Newtonian liquids is larger than for Newtonian liquids with the same apparent viscosity. They also mentioned that this behavior is associated with yield stress of polymeric non-Newtonian liquids which were examined. Other findings by Geckner and Sojka and Lee and Sojka show that spray SMD increases as the liquid viscose-elasticity is increased, either by increasing the polymer concentration in the mixture or by extending the polymer chain.

Influence of liquid physical properties:

Influence of the viscosity on the mean drop size was studied by many workers mostly in range of viscosity from 0.001 kg/ms to 0.968 kg/ms and pressure between 0.2 - 2 MPa. Buckner and Sojka pointed out that mean drop size is independent on the liquid viscosity. On the other hand, findings by Satapathy et al., obtained in higher injecting pressures (11-33 MPa), show strong dependency of drop size on the viscosity. Increase in liquid viscosity causes marked increase in mean drop size.
Other experiments were performed on the influence of the liquid surface tension. In general it can be carried out that in conventional atomizers, spray mean drop size reduced with increase in surface tension.

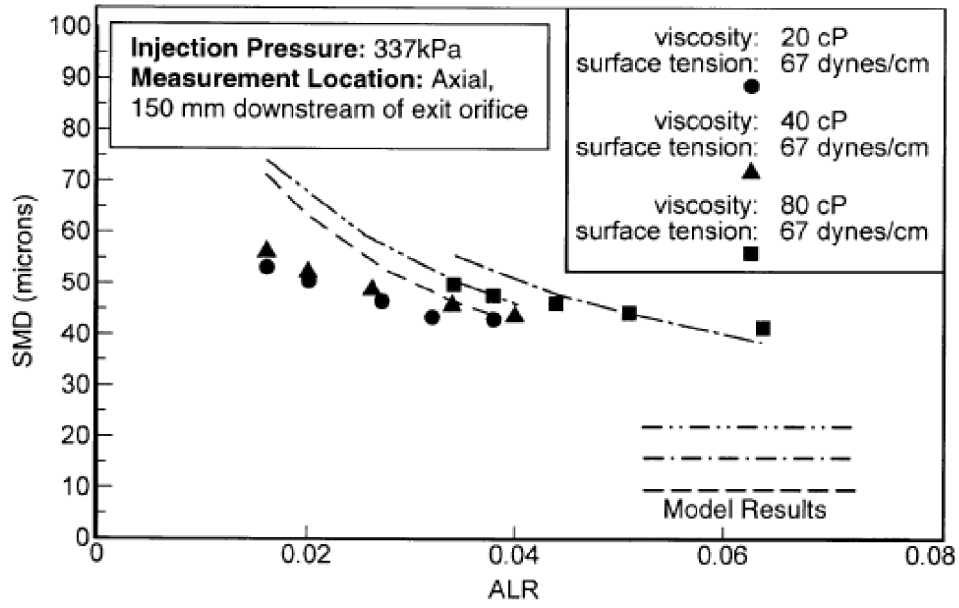

Figure 2-10 Dependency between viscosity on SMD. [5]

Influence of atomizer internal geometry:

Internal design of atomizers has crucial effect on the performance of the atomizer. Several different parameters of the atomizers were studied but only few have demonstrable influence on drop size distribution. As the first parameter is the number of aerator holes is considered. Findings show that narrowed drop size distribution can be achieved using multi-hole aerator in contrast with single-hole aerator with same effective hole area. The next parameter is ratio between exit orifice area and area of the aerator holes (A_o/A_h). In range of lower GLRs (<5 %) low value of (A_o/A_h) causes production of finer spray than atomizers with high (A_o/A_h) parameter. Another parameter of the effervescent atomizers is location of aerator holes. Wade et al. studied that increase in distance of aerator holes from final discharge orifice causes a decrease in mean drop size. This behavior is caused by change of internal flow structure.
The influence on diameter of the final orifice has been studied by several workers but in general the drop size is fairly insensitive to the change in exit orifice diameter.

On the other hand, the length to diameter of the final discharge orifice (*l/d*) ratio has much more influence on the drop size distribution. The findings show that if the (*l/d*) ratio is reduced, the mean drop size decreases.

Influence of the space coordinates:

Whitlow and Lefebvre pointed out that the axial distance has small effect on drop size for low GLRs (<0,8 %) but for higher values of GLR (>1 %) the mean drop size increased up to 20 % with an increase of downstream distance from 102 to 254 mm. This finding is explained as the effect of evaporation and drop coalescence. As well as air-blast and pressure atomizers, effervescent atomizers exhibit slight increase in mean drop size in axial distance from exit orifice in significantly further distance.
Radial distance from the center of the spray was also examined and results are consistent with behavior of other conventional pressure swirl and twin fluid atomizers. The SMD increases as radial distance is increased outward from the center of the spray. This can be described as that the larger drops penetrate further from the center of spray due to their bigger momentum.

3.2 Drop-size distributions of sprays

[2]

The atomizing process has random and chaotic nature. The ligaments formed by the various mechanisms of jet and sheet disintegration vary widely in diameter. Also secondary atomization yields a correspondingly wide range of drop sizes. Most of conventional atomizers produce droplets in the size range from a few microns up to around 500 μm. Only under certain conditions it is possible to create spray, which can be fairly homogenous. Drop size distribution has significant effect on many industrial applications. The most important influence it has is on combustion processes such as the heat transfer, flame length, stability and exhaust emissions. Smaller droplets have a larger surface and therefore it is easier to light-up and results in better heat transfer and leads to improved combustion with respect to flue gas pollutants.

2.6.1. Graphical representation of drop size distribution

[2]

Histograms are usually used to visualize drop size distribution in the sprays. Each ordinate represents the number of drops whose dimensions fall between the limits $D - \Delta D/2$ and $D + \Delta D/2$. Taking into account the weighting effect of the large drops, the histogram of volume is used, see Figure **2-11**. As the value of ΔD gets smaller and provides sufficiently large samples, the histograms assumes the form of a frequency curve.

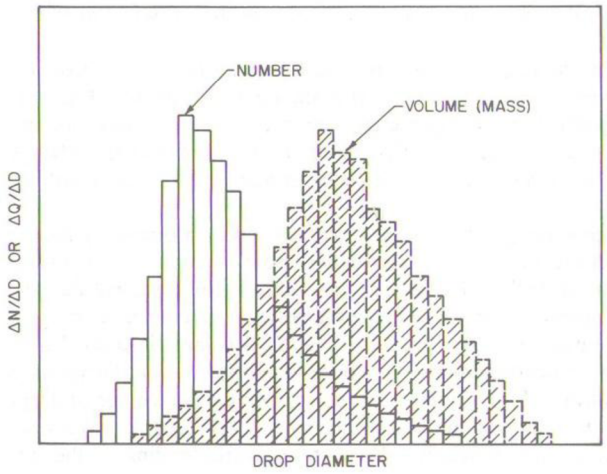

Figure 2-11 Typical drop size histogram. [2]

2.6.2. Mathematical distribution function

[2]

Mathematical functions enable us to predict droplets distribution, which can be obtained from limited number of drop size measurements unlike the graphical representation. Empirical equations are based on probability and experimental considerations. The most frequently used functions are normal, log-normal, root-normal, Nukiyama–Tanasawa, Rosin–Rammler and upper-limit distributions. Every function has it own characteristic field of use that is why it is not possible to use one function to describe all experimental data of droplet sizes. It is recommended to test few functions and pick the best one for given particular application.

One of the most used distribution functions is the Rosin-Rammler originally developed for powders. The distribution is given by the following expression:

$$1 - Q = exp\left(-\frac{D}{X}\right)^{q} \tag{1.1}$$

Where Q is the fraction of the total volume of droplets smaller than D and X and q are experimentally determined constants. Depending on the values of these constants the drop size distribution of the spray can be described. For most sprays the value of q lies between 1.5 and 4. The higher the value of q, the more narrow is the distribution of the drop sizes in the spray. If q is infinite, every droplet has the same size.

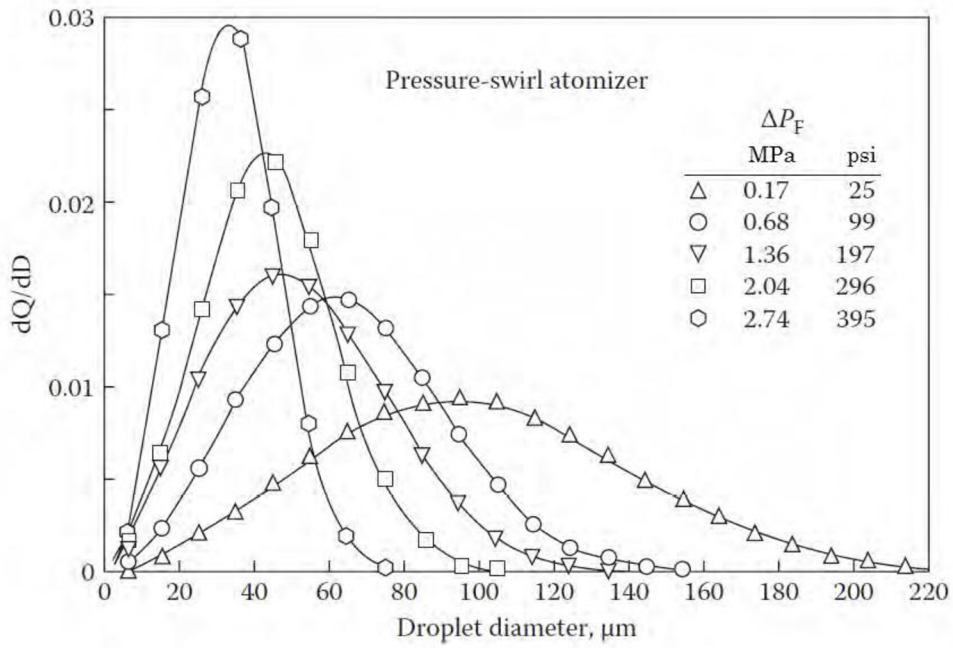

Figure 2-12 Dependence of pressure on the droplet diameter. [1]

3.3 Droplet size

[1], [3]

For the sake of simplicity it is the convention to describe size of drops just with one characterizing number such as mean or representative droplet size. There are many possibilities how to represent droplets diameter. The most widely used diameter for combustion applications is the Sauter mean diameter, for short SMD or D_{32} which is the diameter of the droplet whose surface to volume ratio is the same as that of the entire spray.

To characterize drop size distribution, two parameters are required in most engineering applications. One represents diameter (such as Rosin-Rammler expression) and the other a measure of the range of drop sizes (e.g. standard deviation or q parameter from equation 1.13) In some special cases it may by convenient to introduce another term, such as a parameter to describe minimum drop size. There are other possibilities of representing diameter such as:

- D0.1 = 10% of total liquid volume is in drops of smaller diameter.
- D0.5 = 50% of total liquid volume of droplets are of smaller diameter.
- D0.632 = 63.2% of total liquid volume is in drops of smaller diameter. This is value of X in equation 1.13.
- D0.9 = 90% of total liquid volume is in drops of smaller diameter.

Rosin-Rammler distribution gives us ratios between any two representative diameters as a dependency on parameter q.
Drop size is generally related to design of atomizer, size and operating conditions. And it is highly dependent on physical properties of atomizing fluid. The following Table shows definition of mean droplet diameters and their usage.

Table 1.1.: Mean diameters and their applications.

Symbol	Name of mean diameter	Expression	Application
D_{10}	Length	$\frac{\Sigma N_i D_i}{\Sigma N_i}$	Comparisons
D_{20}	Surface area	$\left(\frac{\Sigma N_i D_i^2}{\Sigma N_i}\right)^{1/2}$	Surface area controlling
D_{30}	Volume	$\left(\frac{\Sigma N_i D_i^3}{\Sigma N_i}\right)^{1/3}$	Volume controlling e.g. hydrology
D_{21}	Surface area – length	$\frac{\Sigma N_i D_i^2}{\Sigma N_i D_i}$	Absorption
D_{31}	Volume – length	$\left(\frac{\Sigma N_i D_i^3}{\Sigma N_i D_i}\right)^{1/2}$	Evaporation molecular diffusion
D_{32}	Sauter (SMD)	$\frac{\Sigma N_i D_i^3}{\Sigma N_i D_i^2}$	Mass transfer reaction
D_{43}	De Brouckere or Herdan	$\frac{\Sigma N_i D_i^4}{\Sigma N_i D_i^3}$	Combustion equilibrium

3. DESIGN OF THE TESTED NOZZLE

One of the aim of this thesis is to design and manufacture effervescent nozzle with regard to the following requirements:

- Simple construction
- Reliability
- Possibility to use various exit orifices
- Possibility to use two lengths of the aerators

The design was conducted by constructions of older nozzles used by Jedelský et al. [6] Aluminum has been chosen for the construction due to corrosion resistance. The assembly drawing is attached in appendix of this work. All drawings were made in Autodesk inventor 2011. With regards to requirements two drawings were designed as the following figures displays:

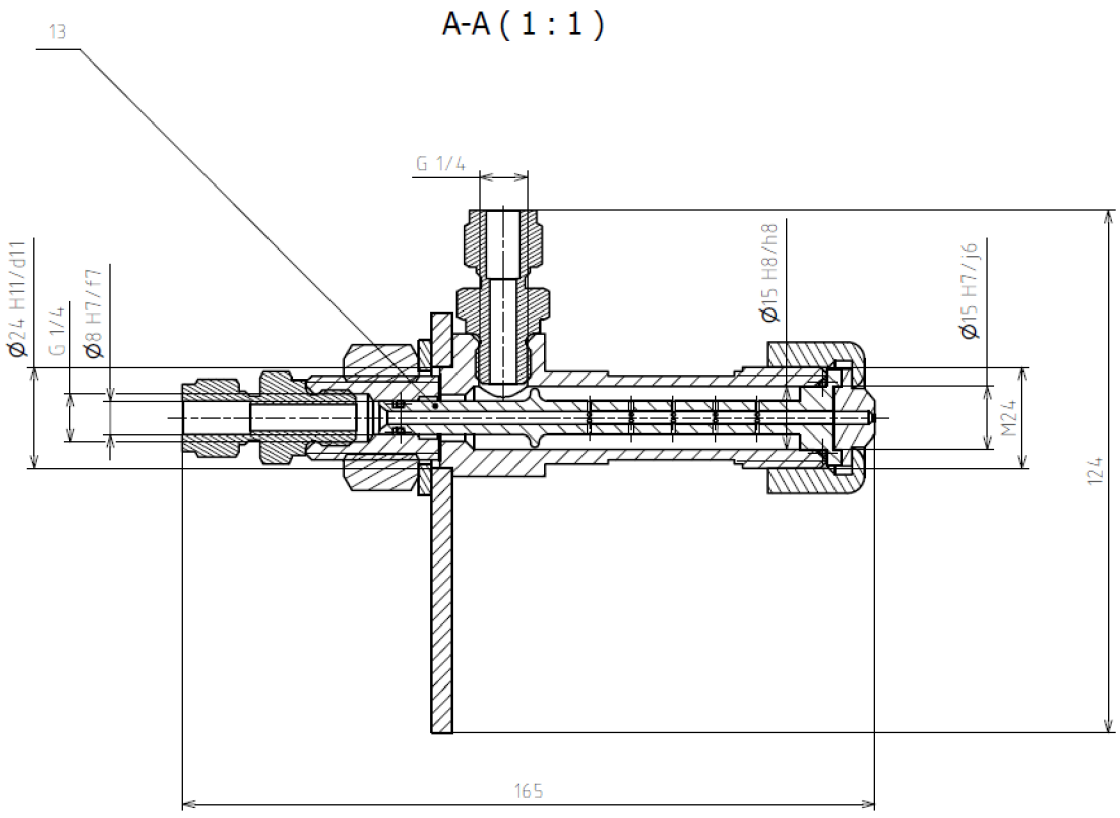

Figure 3-1 Construction for "log" atomizers.

The number of the aerator holes was chosen due to *Ao/Ah* parameter. In long atomizer value of the $\boldsymbol{Ao/Ah = 0.1}$ is given by ten aerator holes with 1 mm diameter and orifice of jet has also 1 mm diameter. On the aerator (position 13) was design a diameter step to compensate air flow along the aerator.

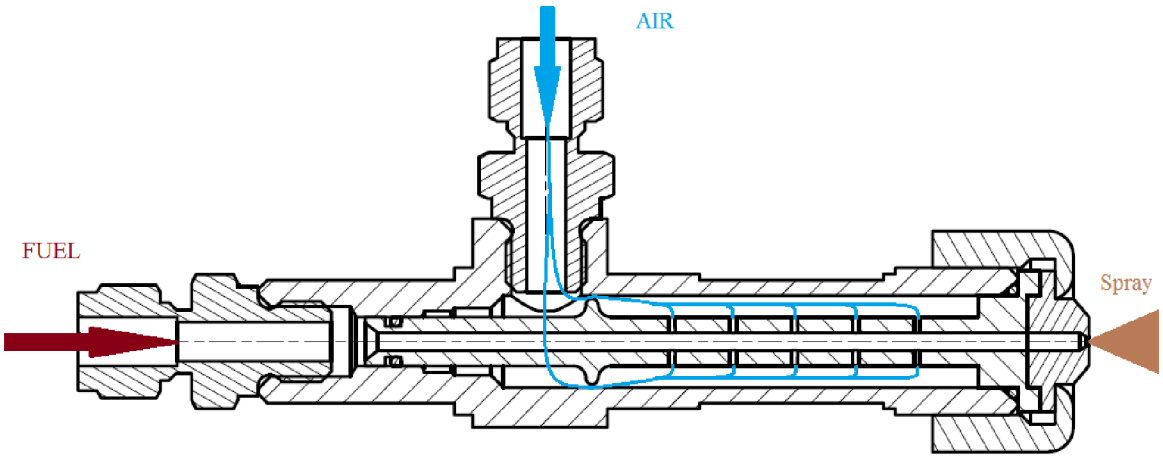

Figure 3-2 Principle of the construction.

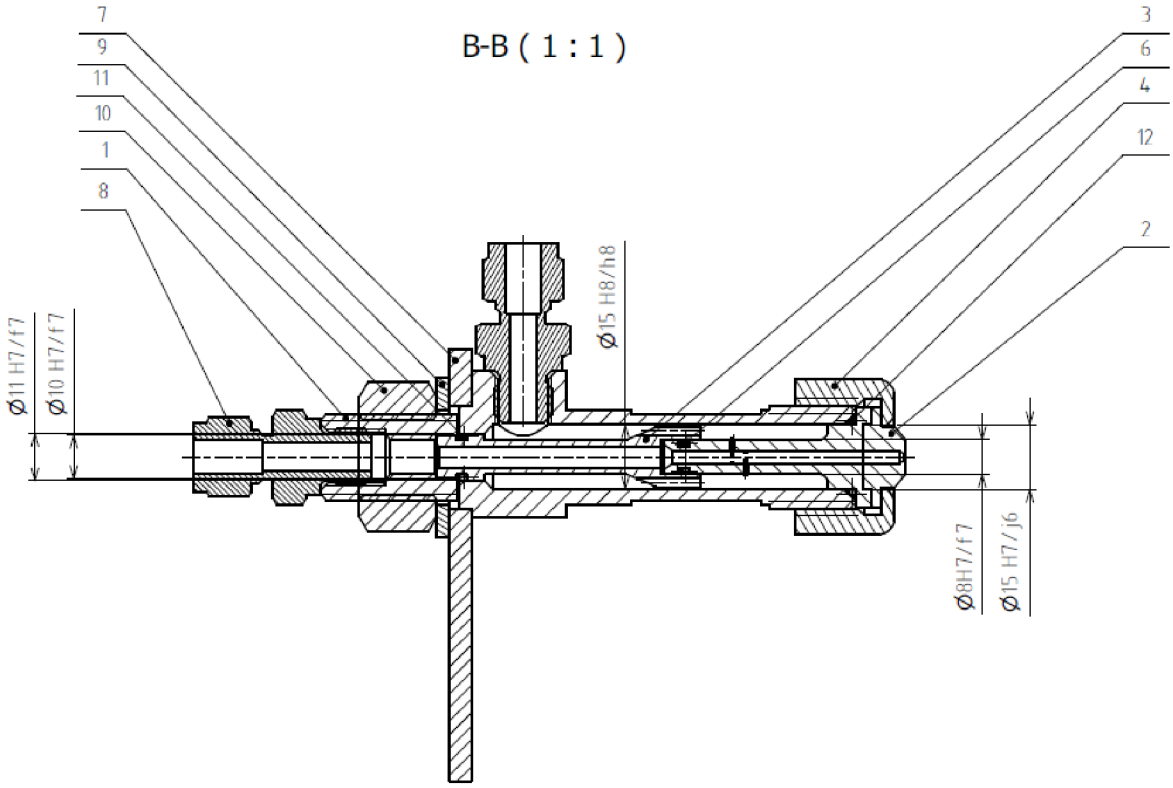

Figure 3-3 Construction for “short” atomizers with reduction part.

The fuel is pumped into atomizers through center hole (position 8 in the Figure **3-3**) and is mixed with air bubbles which are injected into the stream through aerator holes in atomizers (position 3 and 13). Maximum expected liquid flow rate is around 30 kg/h. Maximum expected pressure is around 1 MPa.

The matrix (position 4) enables us to remove and change exit orifices as well as change internal parts. The short aerators fit into reduction part (position 3). The long aerator fits

into Body (Figure **3**-**4**). Every connection (except two parts signed with number 8) is sealed using rubber o-rings. The matrix also has another function. When the matrix is screwed, it pushes parts against each other so all components are pressed together with sealing (positions 6, 11, 12). Body is fitted to the traverse system (position 7) using matrix (position 1) and washer (position 9).

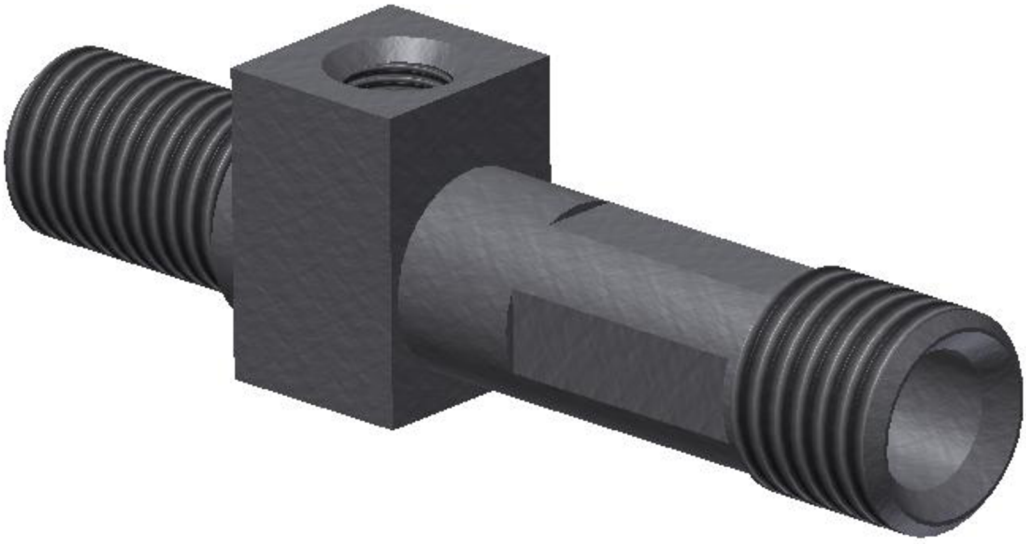

Figure 3-4 Body of the atomizer.

The second jet configuration implements reduction part (Figure **3**-**5**) which enables to use short version of the aerators. It also enables air to get into the aerator holes. That is why it is manufactured with angular grooves and annular holes to decrease hydraulic losses.

Figure 3-5 Reduction part

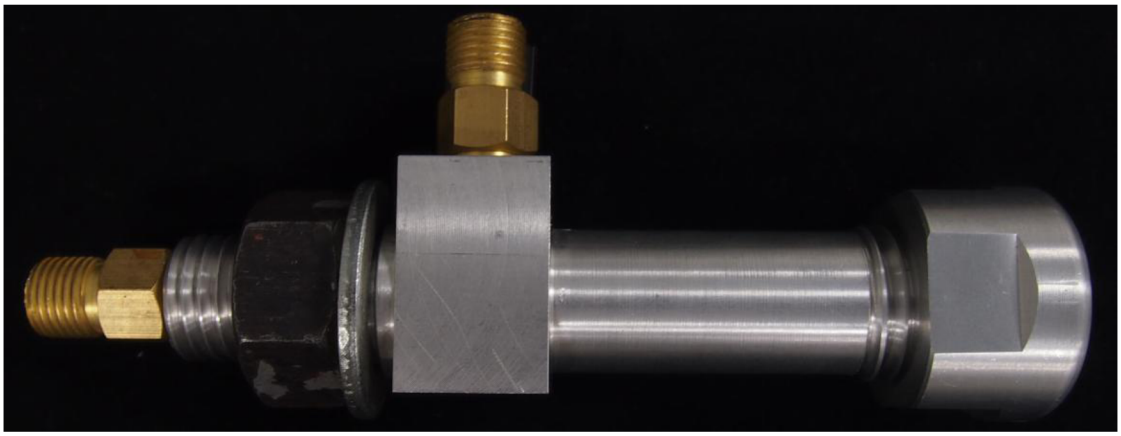

Figure 3-6 Assembled jet

4. LASER ANEMOMETRY

[10], [11], [12], [13]

This part covers principles of laser Doppler anemometry LDA and also extensions of this method PDA (Phase Doppler anemometry) and Dual PDA. They are non-intrusive laser methods for measuring velocities (PDA measures the mean particle diameter) in fluid flows often used in Hydrodynamics, Aerodynamics, Combustion processes or verification of CFD models.

4.1 LDA characteristics

Laser Doppler anemometry enables to measure three velocity components simultaneously. It is an absolute measurement technique with very high accuracy. In comparison with other laser methods, LDA offers unique advantages:

- Non-contact optical measurement – measuring volume is defined by laser beams transmitted from LDA. We measure velocity only with scattered light from particles in fluid. The only limitation of this method is to ensure optical access to measuring volume.
- No calibration, no drift – laser anemometer has a unique intrinsic response to fluid velocity – absolute linearity. The stability and linearity of optical electromagnetic waves could be considered unaffected by other physical parameters such as temperature and pressure.
- Well defined directional response – The quantity measured by the laser Doppler method is the projection of the velocity vector on the measuring direction defined by the optical system.
- High spatial and temporal resolution – we can define a very small measuring volume with LDA optics. Due to this feature we can get a very good spatial resolution. The temporal resolution is given by fast signal processing which permits high bandwidth, time resolved measurement of fluctuating velocities.
- Multi-component bi-directional measurement – using different colors of lasers, polarization and frequency shift allows us to measure up to three velocity channels continuously.

Taking into account these properties the optimization of certain parameters may influence other performance characteristics negatively. In practice some of compromise decisions, which have to be made when setting up the LDA system, can be traced back to the famous uncertainty principle of wave theory.
Due to the small measuring volume, it is necessary to have a traverse system for our measurement to provide measuring in different positions.

4.2 Doppler effect

In general, we can use two different ways to explain the principle of Doppler effect. The description of intersection of two laser beams using definition of Doppler effect and description using a fringe model which commonly used in LDA as a reasonably simple visualization producing the correct result.

4.2.1 The fringe model

If we consider two laser beams which are coherent and if they intersect then they create volume of intersection. In case that those two beams intersect in their respective beam waist, the wave fronts are approximately plane, and consequently the interference produces parallel planes with higher and lower intensity of light. This effect will appear as planes of light and darkness. See **Figure 4-1**:

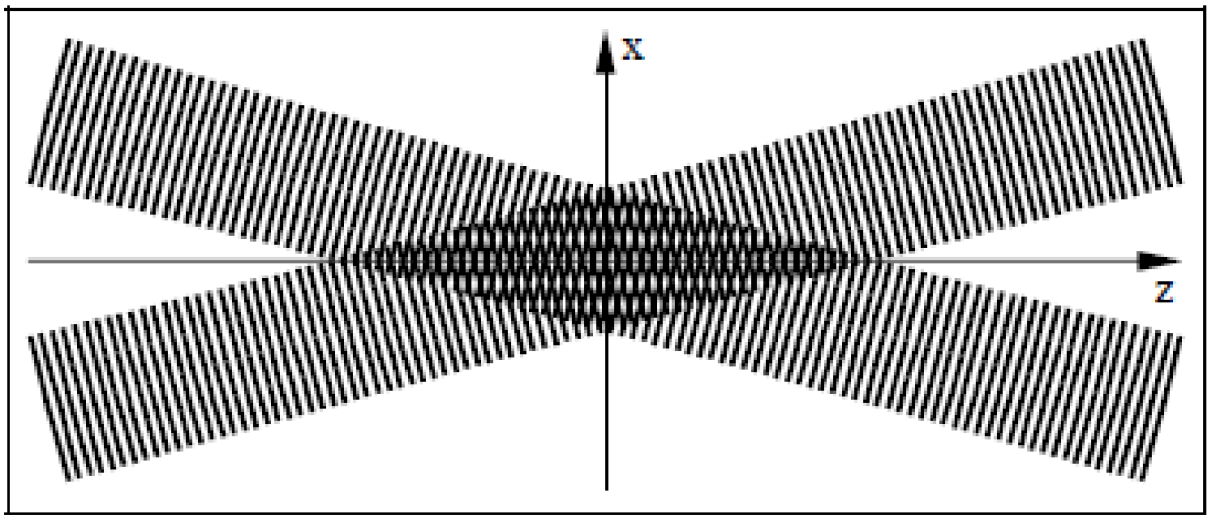

Figure 4-1 Fringe model. [11]

The interference planes are generally known as Fringes. The distance between fringes δ_f is determined by wavelength and the angle between the incident beams. The relationship between those values shows the following equation:

$$\delta_f = \frac{\lambda}{2 \cdot \sin(\theta/2)} \qquad 6.1$$

Where λ is the wavelength and θ is an angle between incident beams. Orientation of fringes is perpendicular to the x-axis. Hence, reflected light from a moving particle through the measuring volume will vary with a frequency proportional to the velocity of particle in x-axis u_x:

$$f_D = \frac{u_x}{\delta_f} = \frac{2 \cdot \sin(\theta/2)}{\lambda} \cdot u_x \qquad 6.2$$

In this relationship, f_D is the Doppler frequency. This equation shows us that if we know a wavelength and angle between beams we can easily calculate Doppler frequency. It is recommended to properly set up laser beams to ensure that beams will intersect in the beam waists. Otherwise, the wave fronts will be curved rather than plane and that could be source of errors in measurement.

4.2.2 Measuring volume

Accuracy and spatial resolution of LDA measurement is given by size of measuring volume. It is dependent on waist diameter of intersecting laser beams and the angle between beams. The measuring volume has an ellipsoid shape due to Gaussian intensity distribution in the beams. Influence of beam waist diameter d_f on the focused laser beams and the angle θ between laser beams is given by equation:

$$d_x = \frac{d_f}{\cos(\theta/2)}; \quad d_y = d_f; \quad d_z = \frac{d_f}{\sin(\theta/2)} \qquad 6.3$$

Where d_x is the height, d_y is the width and d_z the length of the measuring volume.
It should be pointed out that a very small particle in the outskirt of the measuring volume might not reflect sufficient amount of light to be detected. However, if a particle is very large it might reflect so much light, that it is detected even if technically it is slightly outside the measuring volume.
Following equation shows the dependency between number of fringes N_f, height of the measuring volume d_x and fringe spacing δ_f:

$$N_f = \frac{d_x}{\delta_f} = \frac{\frac{d_f}{\cos(\theta/2)}}{\frac{\lambda}{2 \cdot \sin(\theta/2)}} = \frac{2d_f}{\lambda} \cdot \tan(\theta/2) \qquad 6.4$$

This is valid only for a seeding particle, moving straight through the center of the measuring volume along the x-axis. In case a particle crosses through outskirt of the measuring volume then it will pass only less fringes, and consequently there will be less periods in the recorded signal.
It should be mentioned that if we measure with LDA we have to ensure that in the measuring volume there will be a sufficiently high number of fringes. For typical set-up there should be from 10 to about 100 fringes. Measurement accuracy depends on the number of periods, which are generated by the oscillating intensity of the reflected light.

4.3 Frequency shift

The description above describes principle of LDA measuring but with one deficiency. We cannot recognize a direction of velocity of moving particle. The receiver cannot distinguish positive and negative frequencies. Moreover, if a particle moves parallel to the fringes we cannot see any proper signal from the scattered light. That is why Bragg cell is introduced.

The Bragg cell is an acoustic-optical device, which provides a frequency shift to one of the laser beams. It consists of a slab of glass, which has on the one end an electro-mechanical transducer and on the other end has a slab designed to minimize reflection of the acoustic wave. It also absorbs acoustic energy.

The transducer is driven by oscillator which produces an acoustic wave propagating through the glass slab generating a periodic moving pattern of high and low density.

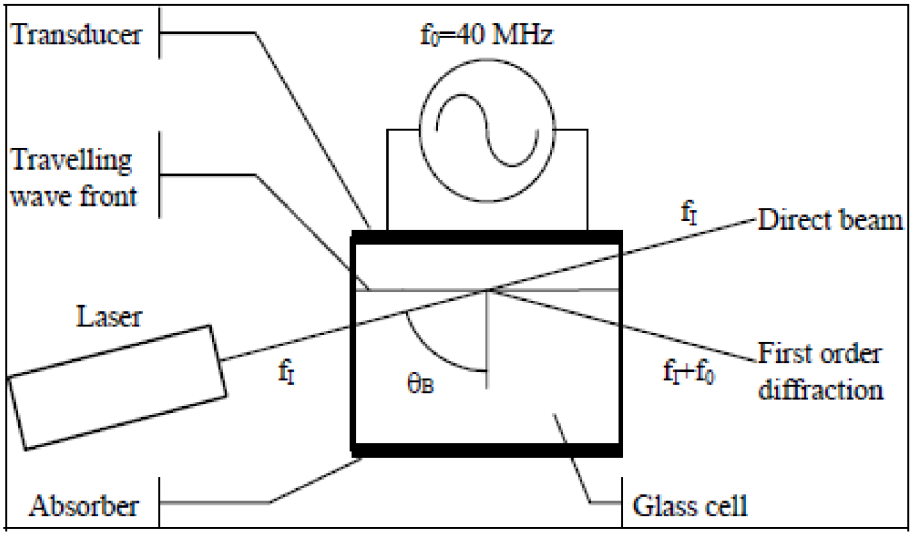

Figure 4-2 Bragg cell. [11]

The incident laser beam comes through the glass and hits a series of traveling fronts. These fronts act as a thick diffraction grid and interference of the scattered light causes intensity maxima to be emitted in a series of directions. In this case, only the first order of diffraction is take into account as an output. The fixed frequency shift (typically 40MHz) is given by Bragg cell to the diffracted beam as shows the following equation:

$$f_D \cong f_0 + \frac{2 \cdot \sin(\theta/2)}{\lambda} \cdot u_x \qquad 6.5$$

Where f_D is the output frequency of the beam, f_0 is the Braggs frequency shift and u_x is the velocity of the particle.

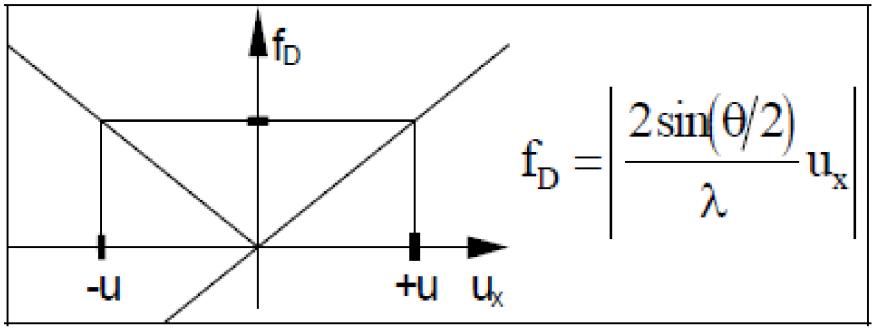

Figure 4-3 Directional ambiguity without frequency shift. [11]

Otherwise, with addition of frequency shift we can calculate velocity without directional ambiguity using relationship:

$$u_x > -\frac{\lambda \cdot f_0}{2 \cdot \sin(\theta/2)} \qquad 6.6$$

The measurable velocities are limited only by response-time of the photomultiplier and condition of signal electronics. Due to those properties, it is possible to get good results even in hypersonic velocities.

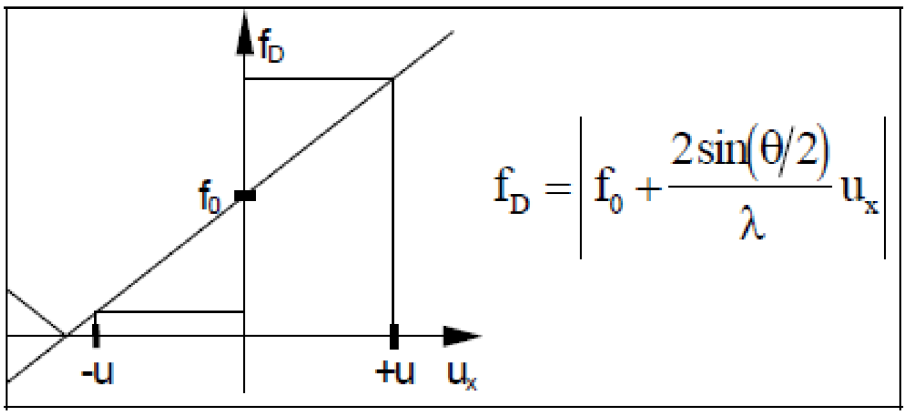

Figure 4-4 Directional ambiguity using frequency shift. [11]

4.4 Lorenz-Mie light scattering theory

This consideration takes into account only spherical particles, and thus describes dependency on particle size, but in general, also shape and orientation of seeding particle has a considerable influence on the scattering of light. As shown in the Figure **4-5** the ratio of forward to backward scattered light can be in the order of 10^2 to 10^3. In general, smaller particles scatter light more evenly than larger particles.

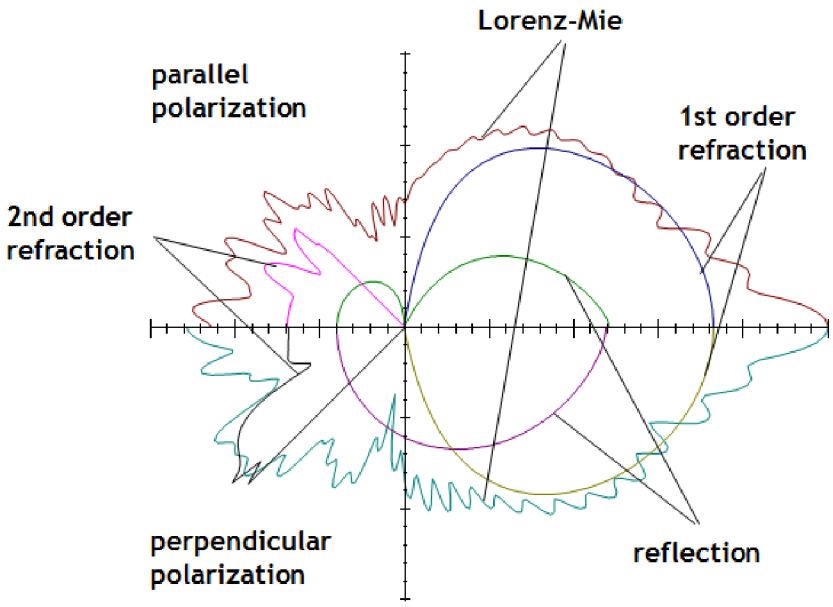

Figure 4-5 Lorenz-Mie scattering theory (the light intensity is shown on a logarithmic scale). [11]

4.5 Backscatter versus forward scatter LDA

Taking into account the Lorenz-Mie light scattering theory, the majority of scattered light is the direction away from the transmitting laser. Much smaller amount of light is scattered to the Transmitter. Thus, forward scattering was used commonly in the early days of LDA. That means that receiving optics was mounted opposite of the transmitting optics. The main advantage of this setting is high light intensity, which is detected by the Receiver.

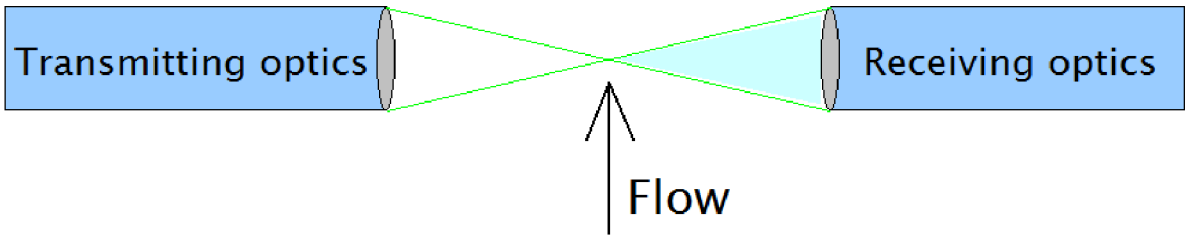

Figure 4-6 Forward scattering LDA.

The backscatter setting was used after some developments in LDA technologies. This is due to much weaker intensity of light, which goes back from the measured particle. Backscatter is much more convenient to set up and today is usual choice for most applications. However, there are still some cases where forward scatter LDA is irreplaceable. For example for high speed flows, acoustic shock waves or very low turbulence intensities.

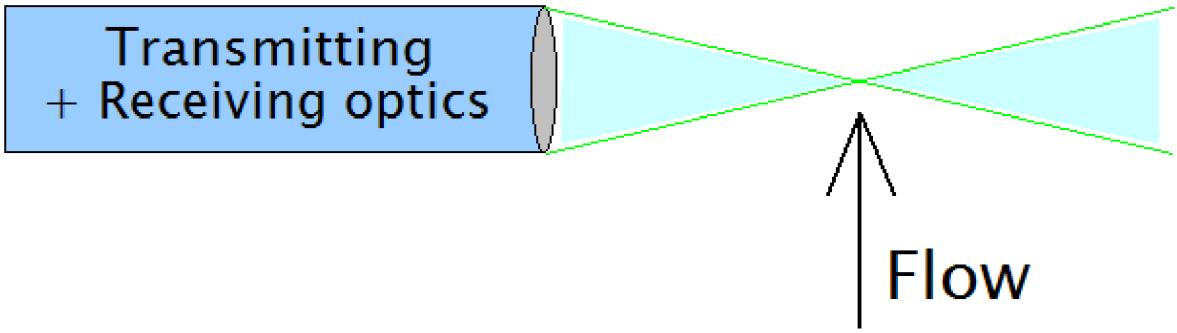

Figure 4-7 Backscatter LDA.

Another position of Receiver is used in LDA measurements. Off-scattering setting is another way to align the Receiver, which is looking at the measuring volume under an angle. This can be a compromise solution in cases where forward or backward scattering is not possible. The position of the receiver causes a decrease in size of the measuring volume as shows the following figure:

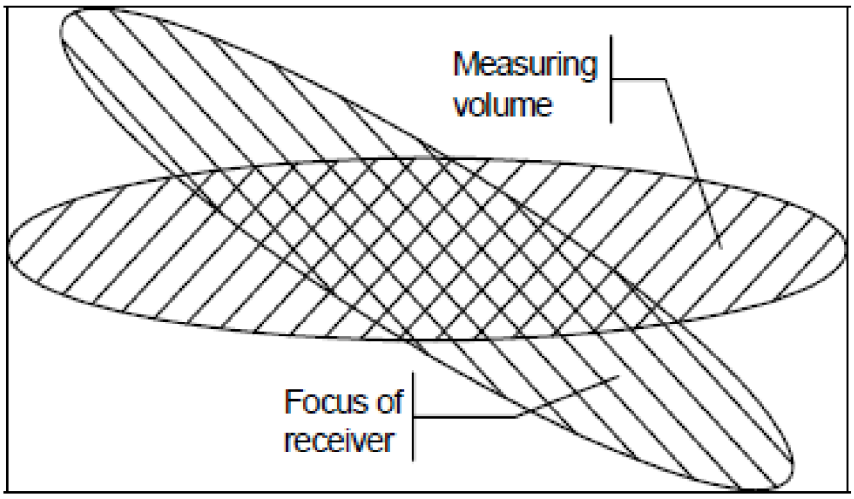

Figure 4-8 Off-axis scattering mode. [11]

Off-axis scattering is preferably used in boundary layer measurements due to smaller measuring volume.

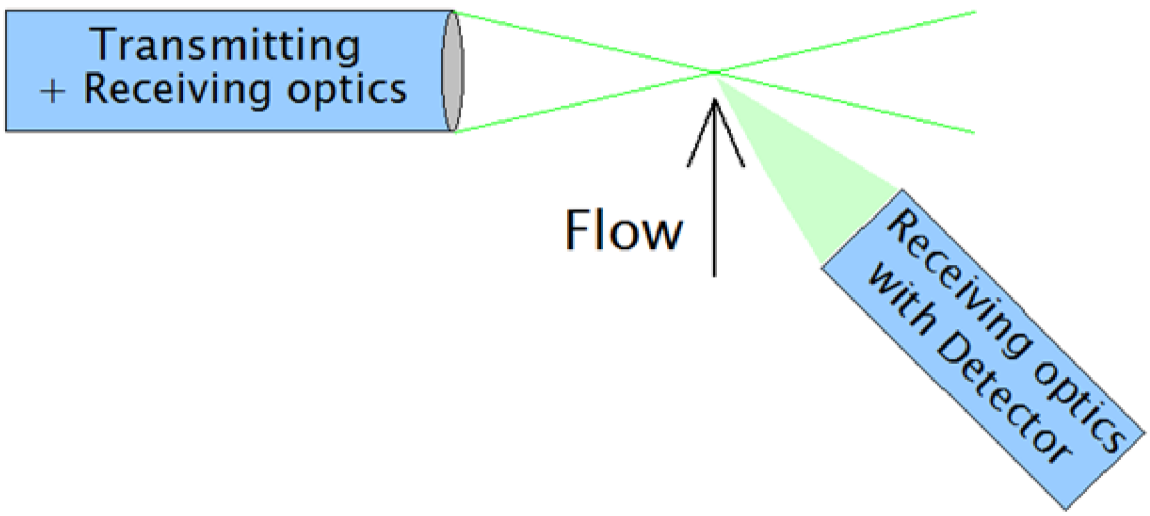

Figure 4-9 Off-axis scattering LDA.

4.6 Phase Doppler Anemometry

PDA method enables us to measure sphericity of the particle in one point on the surface. It also provides measurement of velocity (up to three components), mass flux, concentration etc. This phenomenon was published by Durst & Zaré in 1975 and first commercial instrument was released in 1984.

4.6.1 Basic principles of PDA

It should be pointed out that the difference in optical path length for the reflections from the two incident beams changes with the position of the photo-detector. If we consider that we have two photo-detectors in one receiver then if the particle passes through the measuring volume it transmits a Doppler burst to the Receiver with the same frequency but the phases of the two bursts vary with the angular position of the detectors.

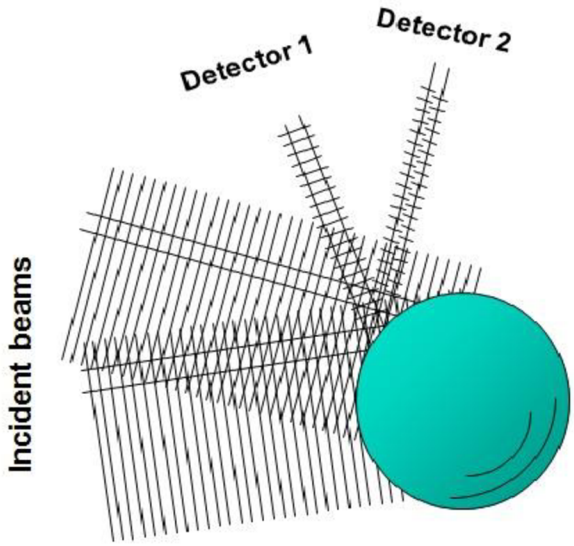

Figure 4-10 The interference patterns differ at the two photo-detectors surface. [11]

4.6.2 Phase-diameter linearity

If the Receiver is in the position that only one scattering mode is dominating then the relationship between phase difference and particle diameter has a linear character.

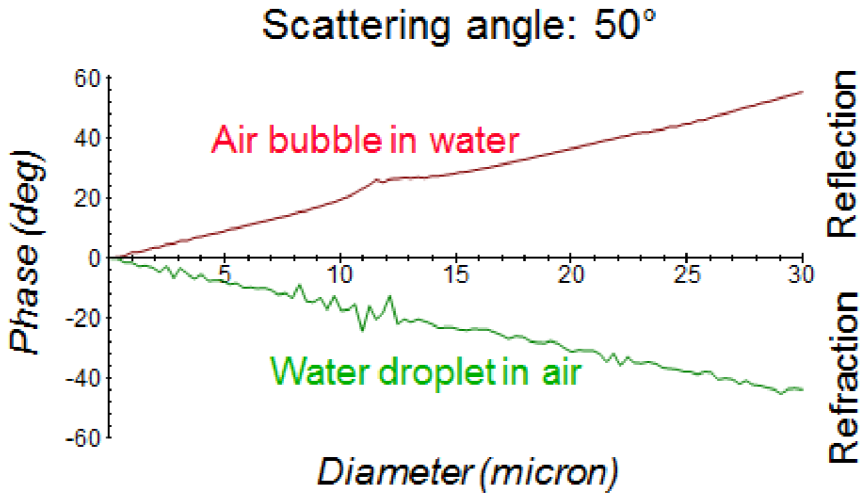

Figure 4-11Phase-diameter linearity. [12]

Non-linear phase-diameter relationship is caused by simultaneous detection of different scattering modes with comparable intensity. It could also be displayed in software as a Phase plot. This gives us valuable information about quality of our droplet size measurements.

4.6.3 Laser beam polarization

Scattering plane is defined by position of Transmitter and Receiver. Polarization is defined relatively to the scattering plane. Parallel (perpendicular) polarization is in the case when polarization is parallel (perpendicular) to the scattering plane. In Figure **4-12**, Y-Z plane is the scattering plane.

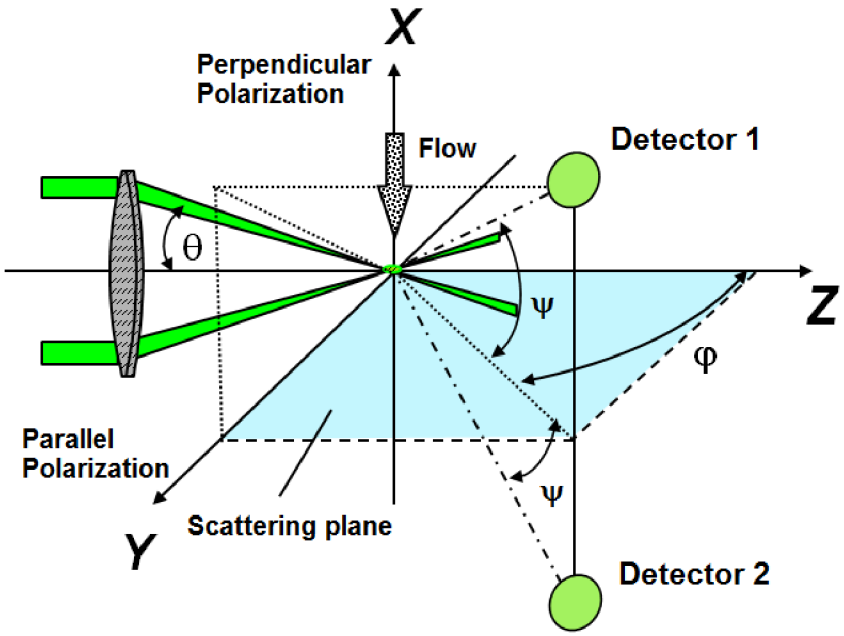

Figure 4-12 PDA configuration. [12]

The geometrical factor β_i between particle diameter and phase shift depends on the scattering angles ϑ_i, ψ_i, φ_i and also on the scattering mode. As shows Figure **4-13** there are main scattering modes. Reflection from outer surface of the particle, refraction through the particle (first order of refraction) and refraction with one internal reflection (second order of refraction). Thus, sensitivity and range of PDA can be altered by changing any of these values.

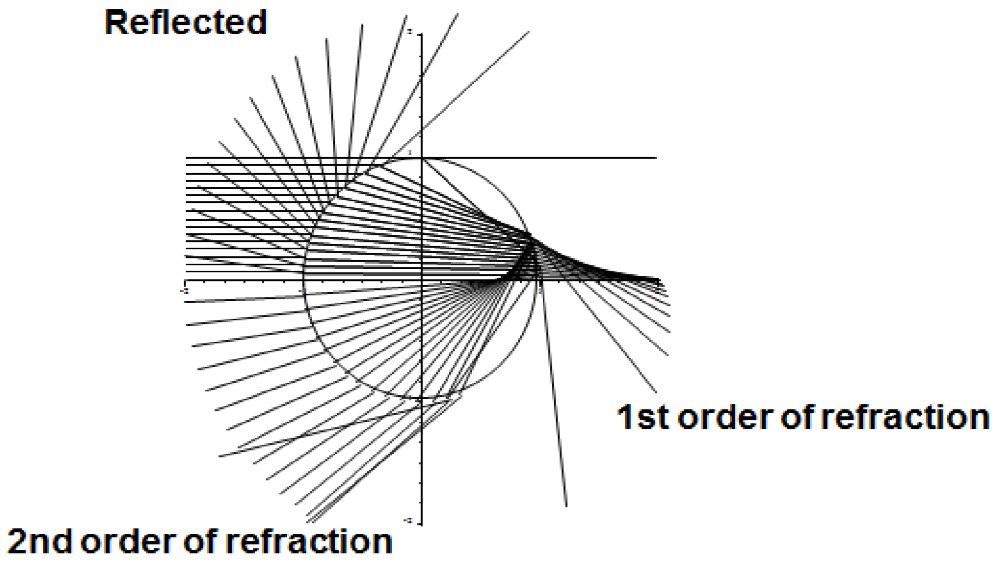

Figure 4-13 Scattering modes (water bubble in air). [12]

4.6.4 Diameter-phase relationship

The phase difference between the two Doppler bursts depends on the size of the particle. As we can see in the Figure **4-14** the burst of the larger particle exceeds that of the smaller particle.

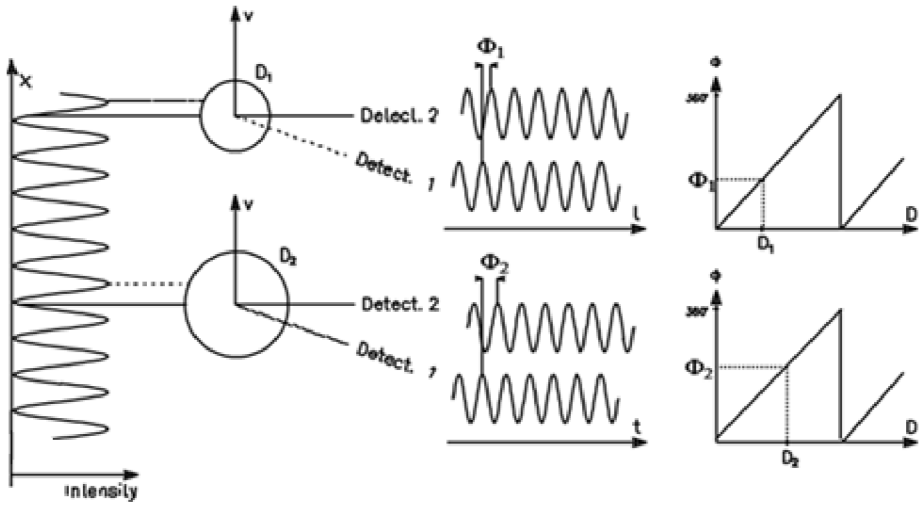

Figure 4-14 Phase difference in relationship to particle diameter. [11]

The phase difference can be calculated from the following equation:

$$\phi_i = \alpha \cdot \beta_i \qquad 6.7$$

where letter i is for detector and the size parameter α is given by:

$$\alpha = \frac{\pi}{\lambda} \cdot D \qquad 6.8$$

where D is the particle diameter and β_i is the geometrical factor. If we consider two spatially-separated detectors the phase difference Φ_{ij} can be calculated as:

$$\phi_{ij} = \phi_i - \phi_j = \frac{\pi}{\lambda} \cdot D \times (\beta_j - \beta_i) \qquad 6.9$$

Where the difference (β_j - β_i) is the phase factor for the two detectors.

4.6.5 2π Ambiguity in two detector system

In Figure **4-15** we can see that too large particle falls beyond the range of 360° (2π). In standard two detector system there is no way to recognize the phase difference between the detectors and thus determine if we measure particle with diameter D'_3 or D_3. This is referred to as the 2π ambiguity.

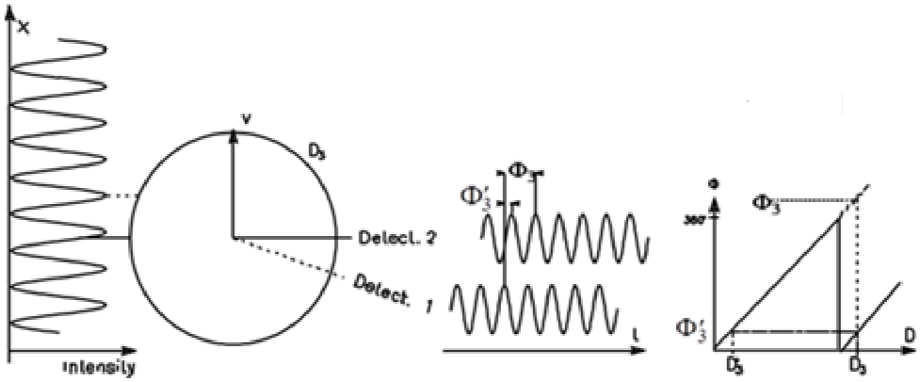

Figure 4-15 2π ambiguity. [11]

To solve this phenomenon the third detector is introduced. That way we get three asymmetrically positioned detectors. The more distanced pair of detectors (usually called as U1 and U2) gives the wider slope of the diameter-phase relationship. Due to this feature the resolution increases and the working range decreases. That is why closer detectors U1 and U3 give smaller slope to the diameter-phase relationship.

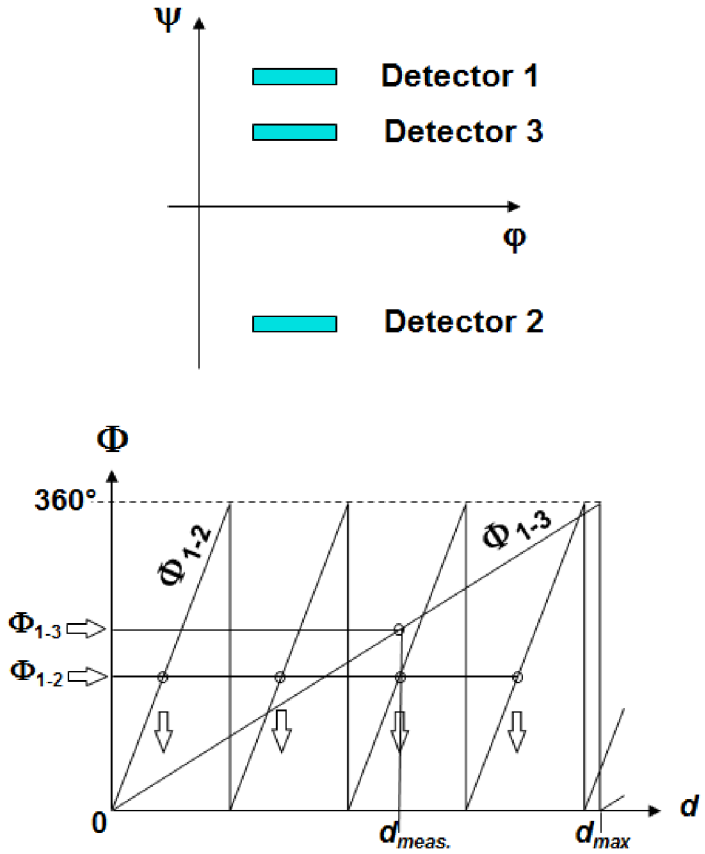

Figure 4-16 Phase-diameter relationship for conventional PDA system with two pairs of photo detectors. [11]

The second useful feature of this two detector setup is information about curvature of the measured particle. Curvature can be determined by the phase difference caused by certain arc of the particle surface. In case that the particle is ideal (spherical) two such pairs of photo-detectors give us the same information about curvature. If we obtain a different signal from detectors we can estimate that the particle is not spherical and thus if the phase difference is too large the particle is not accepted. Criterion for this condition is implemented in PDA software where we can set up value of the maximal allowable deviation from sphericity.

5. TEST BENCH

This chapter describes cold test bench which was used for all measurements. The original design is described in [3]. The part below describes the improvements that have been done for the given application. All added components have been chosen considering their accuracy and measuring range.

5.1 Fuel supply system

Whole fuel supply system is mounted into the mobile frame which enables us to move this system wherever is needed. Copper pipes are used to transport fuel from tank to the exit of the frame. Fuel supply system consists of two circuits. The first pushes fuel into the heat exchanger which is connected with Chiller to keep constant temperature of fuel. It also provides possibility to set the temperature of the fuel to a specific value. To transport fuel from tank to heat exchanger a diaphragm pump is used.
The second circuit pushes fuel into the nozzle. The main part of the fuel supply system is gear pump placed at the bottom of the stand. It draws fuel from fuel tank through filter and pushes fuel through regulation valve to Coriolis flow meter. Behind the mass flow meter a valve, pressure sensor and temperature detector are mounted. Then fuel is pushed into the nozzle.
Fuel is sprayed into the collection chamber and from this point it flows down due to gravity back into the fuel tank. Connections are assembled by Swagelock fittings due to their reliability. Schematic layout of the testing bench is shown in the following figure:

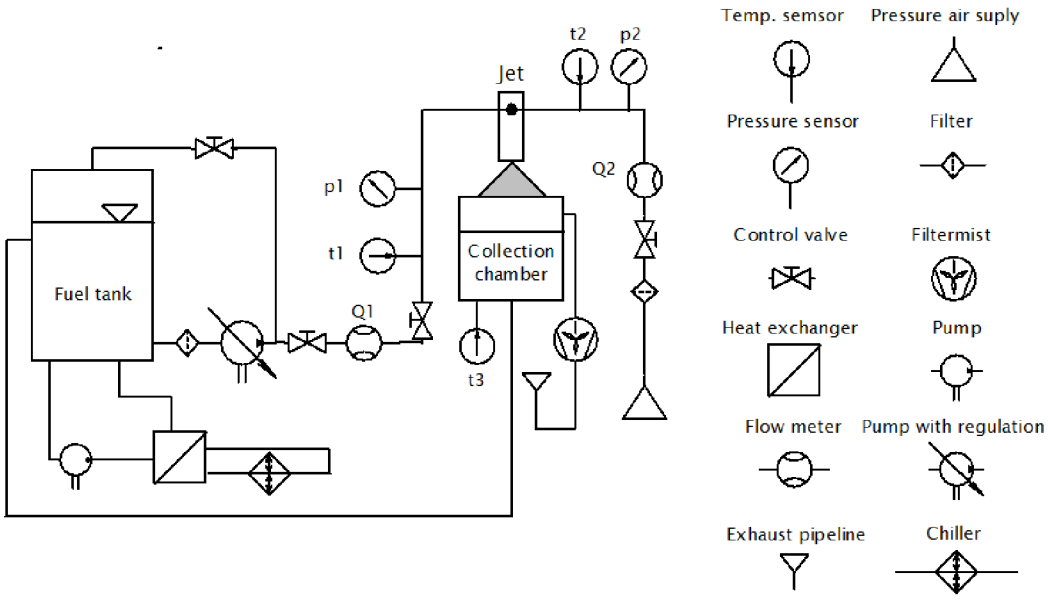

Figure 5-1 Test bench.

Pump control is performed by changing motor power input and using bypass loop and two regulation valves. The first valve is fitted in bypass loop and second is mounted next to the flow meter.

5.1.1 Flow meters

For measuring mass flow in fuel loop, a Siemens Mass 2100 Coriolis flow meter was used fitted with Mass 6000 Ex transmitter. This flow meter provides accuracy ±0,1 % of the indicated value. Operating range for this meter is 0-250 l/h. [14]

Air flow was measured using Omega FMA A2311 with ±1 % accuracy of full scale at operating conditions. Mass flow range is 0-20 SLPM. [15]

5.1.2 Temperature

In the test bench three resistance temperature detectors SPRTX-S1 by Omega were mounted to provide detailed information about atomizing mixture. As was mentioned earlier one detector was fitted in fuel loop and the second one was mounted in air loop and the third detector was placed into the collecting chamber to measure temperature of the atomizing spray (see Figure 3-4). Operating range of these detectors is -99 to 208 °C. Accuracy of this sensor is ± 0.5 °C of full scale. The output is 4-20 mA. [16]

5.1.3 Pressure

In the test bench two BD sensors DMP 33li with range of 0-18bar in each loop were mounted. Accuracy is 0.1 % of full scale. These sensors have linear current output 4-20 mA. [17]

Signal from each sensor was processed in program created in LabVIEW, which was designed especially for this application. Program available on attached DVD.

5.2 Pressured air supply system

Air is taken from the central pressured air system. Maximum pressure is about 0.8 MPa. Air comes through dehumidifier and filter into regulation valve. Pressure and temperature sensor is mounted in air branch as mentioned above.
Air is mixed with fuel in mixing chamber in the nozzle. Air comes through aerator holes in aerator and creates bubbles in fuel flow and expands into ambient air.

5.3 3D traverse system

For spray measurements with PDA method it is necessary to be able to measure in different points in the spray. That is why traverse system is introduced. This system enables us to change positions with the smallest step of 0.05 mm. Range of this system is 300 mm in each direction.
In some applications of PDA it is common to travers with optics instead of the nozzle. Especially in cases where it is not possible to move with measured area such as measurements in combustion chamber and so on. The tested jet was mounted on clamp which was mounted on the motor of the Travers system. This setup was assembled due to spatial options of the laboratory and previous designs.

6. EXPERIMENTAL SETUP

6.1 PDA measuring system

[11]

For measurement the 2D Fiber PDA system by Dantec Dynamics was used. System consists of:

- Spectra physics Stabilite 2017 Argon laser: maximum power output 6Watt.
- 60X41 Transmitter: Transmitter splits the beam into its individual color components (476,5 nm, 488,0 nm, 514,5 nm) and divides each color into two beams. Also Brag cell is implemented in this device which gives frequency shift 40*MHz* to each beam from given pair.
- 60X81 2D 85 mm Transmitting optics with 50X82 Beam Translator which provides fine adjustment of beam intersection. It is useful in applications with limited optical access.
- 57X50 112 mm diameter fiber PDA receiver optics with spatial filter
- Fiber PDA Detector unit
- BSA P80 Flow and Particle Processor

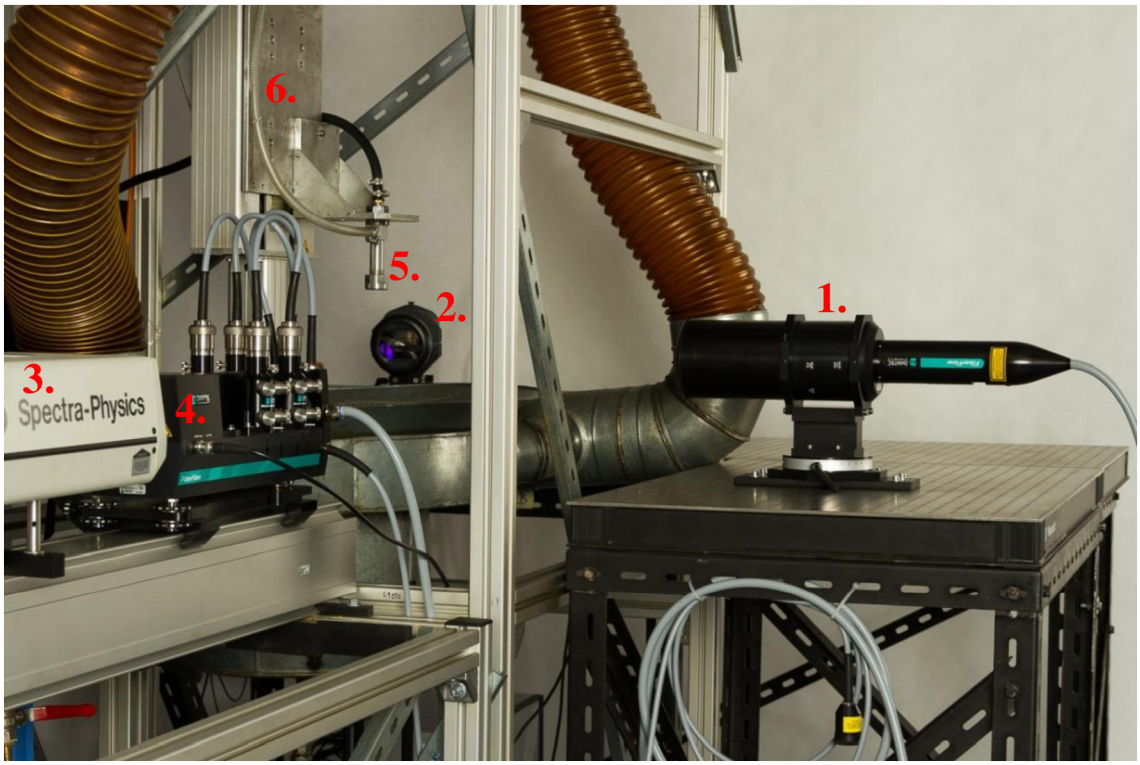

Figure 6-1 Photograph of PDA layout:

1-Transmitting optics, 2-Receiving optics, 3-Ar-Io Laser, 4-Transmitter, 5-Nozzle, 6-Travers system

Focal lengths were chosen 500 mm for transmitting optics and 800 mm for receiving optics due to optical access to the center of the spray. The half-intersection angle between the beams is 4,303°. Dimensions of the measuring volume are dx = 0.1166 mm, dy = df = 0.1162 mm, dz = 1.549 mm. The scattering angle (angle between Transmitting and Receiving optics) was set to 69°. The beam diameter was 1,35 mm.

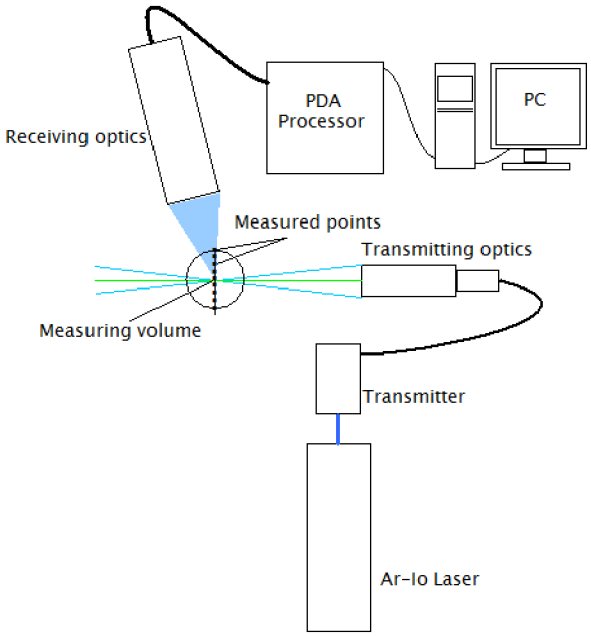

Figure 6-2 PDA schematic layout.

6.2 Description of setting up the PDA system

6.2.1 Laser setup

[19]

Laser is the main part of whole PDA system. It determines beam power and it has influence on light intensity distribution of the beam. An Argon laser can provide the following single line wavelengths:

Table 6.1.: Single laser wavelengths

514,5 nm	488,0 nm	465,8 nm
501,7 nm	476,5 nm	457,9 nm
496,5 nm	472,7 nm	454,5 nm

Optional setup of the laser can be achieved by aligning high reflectors (rear and front mirrors). The mirror must be perpendicular to the beam for optimum performance. The power output should be controlled using accurate motion screws. We can find optimal setup which is signed by the highest possible power output of the laser.
The used laser further enables us to change apertures which determines diameter of the output beam diameter.

The laser is controlled by remote Controller. It can be running on Power or Current mode. Generally, Power mode has more stable power output but for detailed view of the laser condition Current mode is used. Usually misalignment of the high reflector causes increase in current for required power output.

Laser beam comes from laser head to the Transmitter box. Where *Brag cell* and *Color splitter* is implemented. Color splitter splits the incoming laser into its individual colors (their wave lengths see Table 6.1.). Transmitter box enables us to control energy for each beam (shifted and un-shifted for each color) using *Level adjust*. The beams passe through Transmitter box into *Manipulators* where they are focused into light cables. The efficiency of the Transmitter box is around 80% and efficiency of the light cables is slightly more than 50% depending on the Manipulators alignment. For 1 W laser power coming from laser head we can get around 120 mW on green beams and around 100 mW on blue beams.

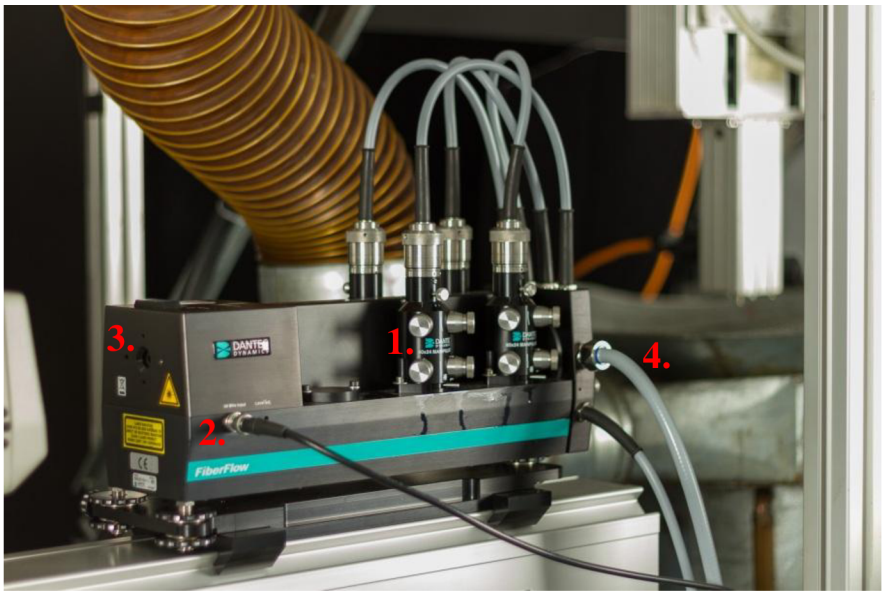

Figure 6-3 Transmitter box:1-Manipulator, 2-Frequency shift input, 3-Laser beam input, 4-Output optical cable.

For the first alignment of the Manipulators it is recommended to decrease the laser power to the minimum and find optimum setup using accurate screws. The quality of the setup is controlled by laser power output. It is an iteration process and it can change in time due to physical properties of ambient environment like temperature and humidity. It is

recommended to check alignment of the manipulators before each measurement to ensure quality of the setup.
It should be mentioned, that the laser systems are very sensitive and it should be operated very gently with them. It is recommended to measure laser power output often to control laser condition in time. Any rapid decrease in laser power output signs fault in laser or misalignment of the laser mirrors.

6.2.2 Settings of the optics

Receiving and transmitting optics must be focused into one point (Measuring volume). First of all, both optics must be mounted in one horizontal plane. Transmitting optics enable us to change angle between optics and table. It also enables us to change lenses therefore change focal lengths. Beam direction is controlled by Beam translator. Beam intersection point must be the same for all four beams. This point can be controlled using Dantec PDA camera. The **Figure 6-44** shows typical position of two laser beams obtained by camera.

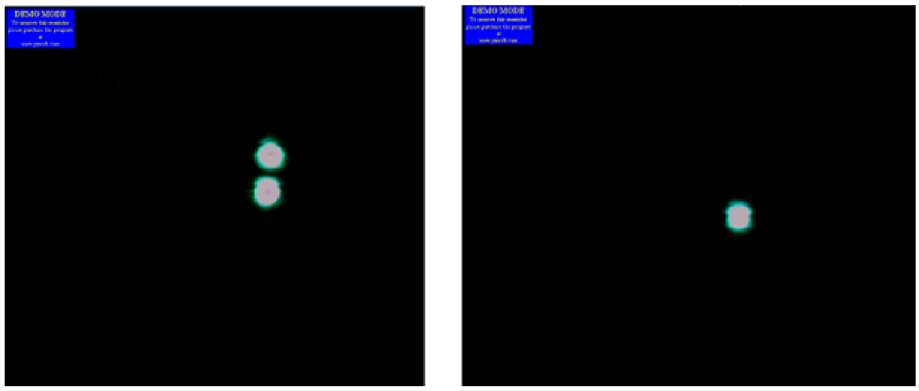

a) b)

Figure 6-4 Beam alignment.

In **Figure 6-4 a)** shows two beams out of the measuring volume. **Figure 6-4 b)** shows two laser beams which intersects in measuring volume.
The position of laser beams in measuring volume has crucial effect on bursts created by flowing particles and thus on the results on whole measurement. The wrong setup of the beams causes deformation of the measuring volume and thus erroneous measurement.

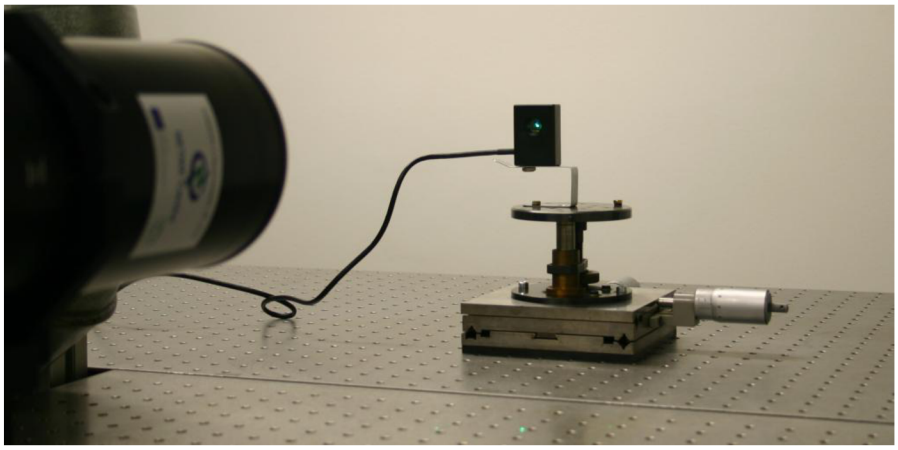

Figure 6-5 Setting up beams with PDA camera.

Horizontal position of the beams should be set precisely. Even small tilt of the Transmitter causes inclination of the fringes to the optimal horizontal plane and leads to incorrect results of velocity distribution in the spray. This setup can be controlled using spirit level and it can be also shown on results of the known spray.

The used system enables to change position of the Receiver (angle in horizontal and vertical plane, distance from the measuring volume and direction perpendicular to the axis) using motion screws. For fine adjustment the eyepiece (placed in the Receiver) is used. With this device the direction and distance (from measuring volume) of the Receiver can be set by evaluating the view focusing. The position of the view must be focused into the point where beams cross.
To ensure the quality of the hardware setup an Oscilloscope is often used. It should be connected with PDA processor so we can see the signal even before it is processed by processor. We can judge the shape and phase difference between signals from green and blue laser beams. If we can see phase shift between bursts it signs that measuring volume of the one color is not in coincidence with another color. We can find the optimal position of the Receiver by judging the maximum amplitude of bursts.
Another way, how to judge quality of hardware settings is to use Phase plot. It displays relationship between two measured phase differences (U12 vs U13). It is mainly used to facilitate proper optical alignment of parameters which influence the particle size measurement. A typical Phase plot is shown in the following Figure:

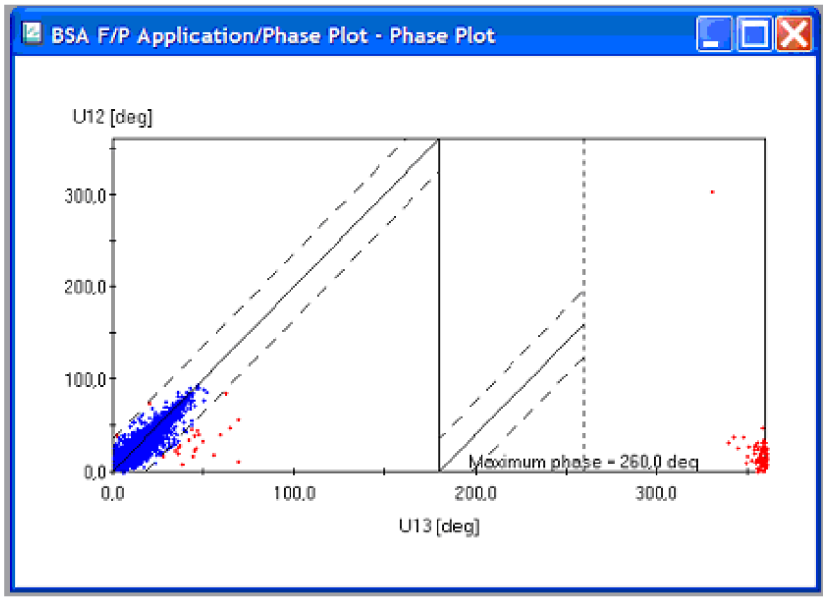

Figure 6-6 Typical Fiber PDA phase plot. [11]

The diagonal continuous line stands for denoted photo-detectors relationship for ideally spherical particles. Two parallel dashed lines show deviation from ideal line (called Phase validation ratio in software). It can be set by user for given case. For our measurements the value of the Phase validation ratio was set to 10%.
The colored dots in Phase plot display measured particles. The blue (or green) dots are valid samples and the red dots are rejected samples. The valid samples are inside acceptance band.
Usually they is only a small amount of red dots in Phase plot. But poor alignment or poorly set parameter in software can cause a deviation from optimal distribution. Using information from PDA manuals we can estimate possible fault from Phase plot.

6.2.3 Software settings

[11]

For the first calibration it is recommended to use spray with known drop size distribution and droplets SMD. Used PDA system was tested on the LHO spray produced by Air-brush nozzle.
For all measurements BSA flow software v5.1. by Dantec. was used. After Hardware adjustment it is necessary to find the best setting for the software. The main characteristics which have influence on the quality of the results are:

- Sensitivity of the photo-detectors: The increase of the sensitivity causes higher Data rate, but overlapped settings have a negative influence on the Phase plot (giving more signal from different refraction modes in droplets).

- Signal gain: Gain amplifies signal from photo-detectors. Higher Gain leads to higher Data rates but smaller Validation due to higher SNR (signal to noise ratio).
- Record length: Determines record interval. There are two regimes. In Auto adaptive mode processor will adapt record length to each burst. In Fixed mode only one record length is always used.
- Velocity span: It determines range of the measured velocities of the particles. It should be set according to expected flow velocity. It is possible that in case of the small ranges, every particle cannot be measured. For first settings it is recommended to set wide Velocity span to determine whole velocity distribution.
- Velocity center: Sets center of the measured Velocity span. It should be chosen according to expected flow velocity.

Whole setup is an interaction process. It is necessary to setup PDA system for each spray individually.
Measurement quality is also influenced by laser power output. In cases where we need stronger signal, for example Phase plot indicates that we do not see smallest particles in spray. It is recommended to control laser power more than to change the sensitivity of photo-detectors due to SNR value.

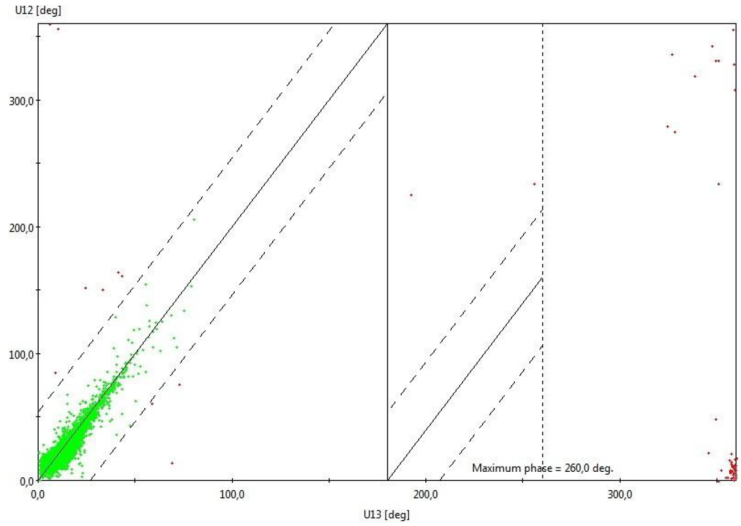

Figure 6-7 Phase plot obtained by Airbrush measurement.

As was mentioned above the Phase plot is a tool which shows quality of PDA setup (Hardware and Software). The **Figure 6-7** shows Phase plot obtained by airbrush with LHO as an atomizing fluid. Important on this plot is that we can measure the smallest particles. It is signed by the amount of green dots at the low left corner. There are also some red dots (invalid samples) but it is only negligible amount. From this point of view, we can estimate that our setup is well performed.

6.2.4 Measurement settings

Before final measurement it is necessary to make measurements in areas and regimes of our interest to estimate the velocity center, velocity span (for each channel LDA1 and LDA4) and for particle diameter span. Histograms show velocity and particles diameter distribution. Crucial for setup are borders of measured spray (where are the lowest velocities and the biggest particles) and the center (where on the contrary are the highest velocities and the smallest particles). The typical Histogram from measurement is shown in Figure **6-8**.

For all measurement velocity span for LDA1 (axial velocity) was set to 38,57 m/s, velocity center to 14,45 m/s. For LDA4 (radial velocity) velocity span was set to 36,59 and velocity center was 0 m/s.

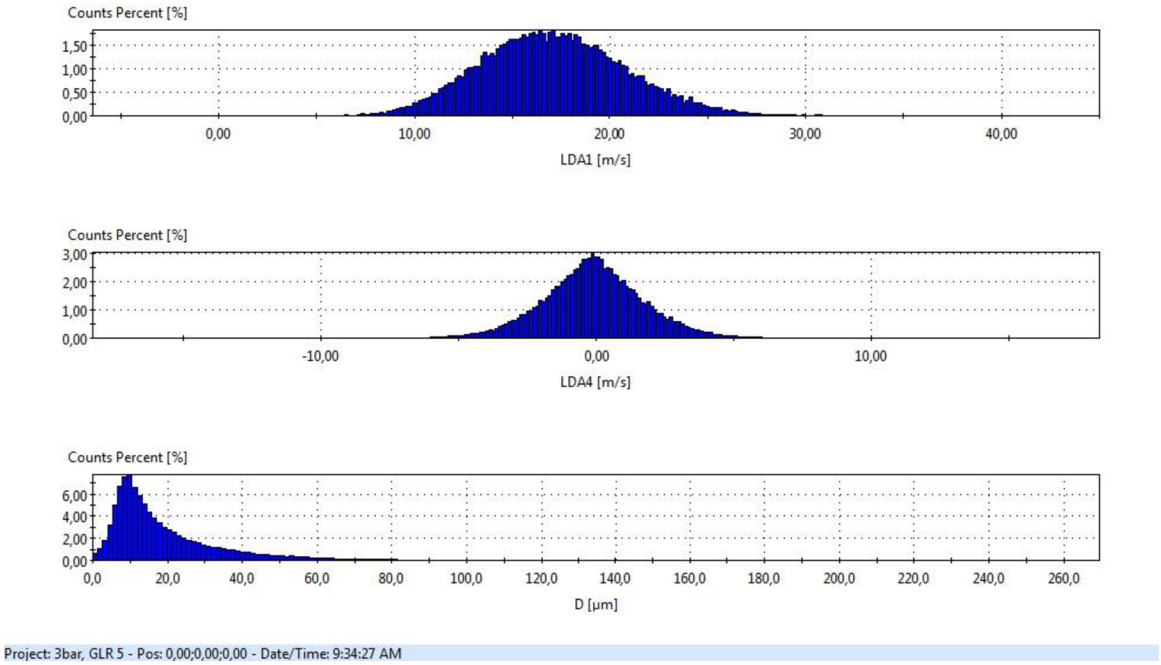

Figure 6-8 Typical histogram.

To judge quality of our setup Phase plots were controlled. As we can see in Figure 6-7 the Phase plot has many red dots. After checking all hardware components, settings and software setup, no fault was observed. The reason of why the Phase plot looks like this is probably due to unusual spray behavior which is in detail described in the Chapter 7. This spray produced pulsations which do not have spherical shape. Thus, linearity between U13 and U12 is not respected. Further, high laser power can reflect light from large particles which are crossing the edge of the measuring volume and thus give invalid samples. The atomizing LHO has relatively high density and is also luminescent. These properties might have influence on PDA measurement and influence the Phase plot. The optical access to the measuring volume through dense spray might cause higher signal noise.

The red dots can be reduced by decreasing laser power or sensitivity of the photo-detectors, but in that case we will not be able to measure smallest particles. They will not be able to reflect a strong enough light signal.

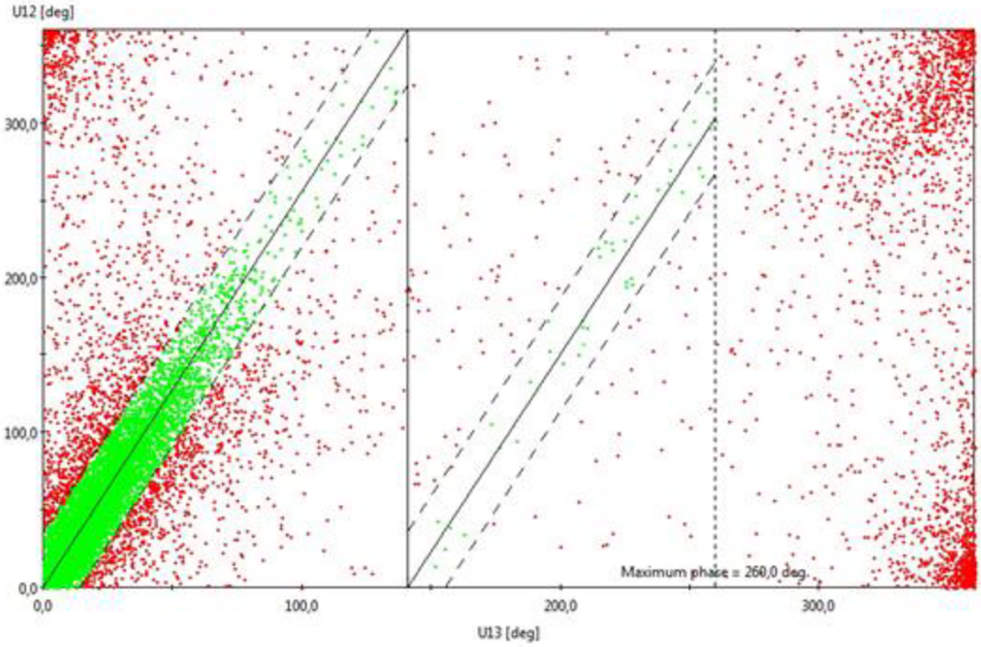

Figure 6-9 Phase plot for effervescent jet.

6.3 Atomizing liquid

The atomizing liquid was Light Heating Oil (LHO). Viscosity was examined by changing liquid temperature using Chiller (described in Chapter 5). Kinematic viscosity is dependent on the liquid temperature according to the following equation [20]:

$$\nu = A_1 \cdot \exp\left(\frac{Ev}{k} \cdot T\right) \tag{6.1}$$

Where k is Boltzman's constant, T is the Temperature and A_1 and Ev are constants. Kinematic viscosity ν for LHO at standard conditions (20°C) is $2.12e^{-5}$ m^2/s. This corresponds to value of $A_1 = 3.41e^{-11}$ m^2/s and $Ev/k = 3908.7$ K^{-1}. Dynamic viscosity μ can be calculated using equation (1.4).

According to equation above viscosity at temperature 15°C can be determined. The values of viscosity are writen in the following table:

Table 7.1. The physical properties of the examined Light heating oil.

Fluid	μ [kg·m^{-1}·s^{-1}]	ρ [kg·m^{-3}]
LHO (15°C)	0.0233	877.6
LHO (20°C)	0.0185	874
LHO (21°C)	0.0176	873.4

Air was used as atomizing gas. The temperature was controlled at a value of 20°C for all measurements. Physical properties are written in the following table:

Table 7.2. The physical properties of atomizing gas.

Fluid	μ [kg·m^{-1}·s^{-1}]	ρ [kg·m^{-3}]
Air	1.82×10^{-5}	1.23

7. RESULTS

This chapter describes results from measurement of effervescent jet. Construction of this atomizer is described in Chapter 3. Whole results were obtained using Dantec Fiber PDA system described in previous chapter.

7.1 Visualization of spray

For the first estimate of spray behavior photos of each flow regime (GLR and pressure) were made. The layout of the camera setup is show in the Figure **7-1**. The mirror was used to improve lighting of the spray from both sides. The camera Canon 300D and objective Canon EF 100mm f/2.8 USM Macro were used for all photos. The Exposure was set to 9 and Shutter speed was 1/4000 s. For lighting an external Flash camera was used.

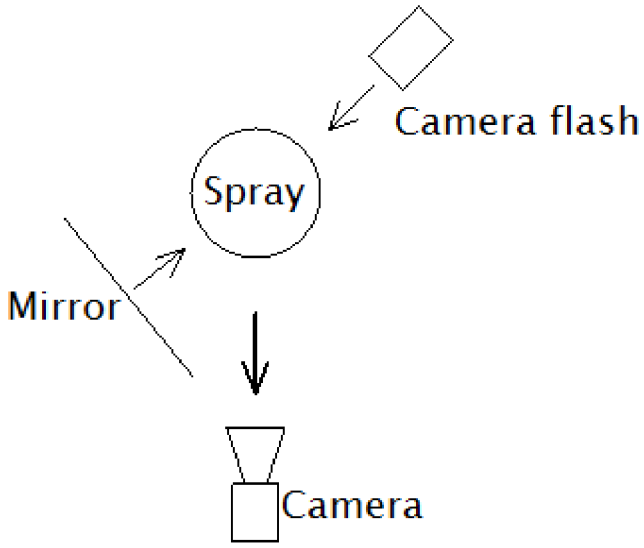

Figure 7-1Camera layout.

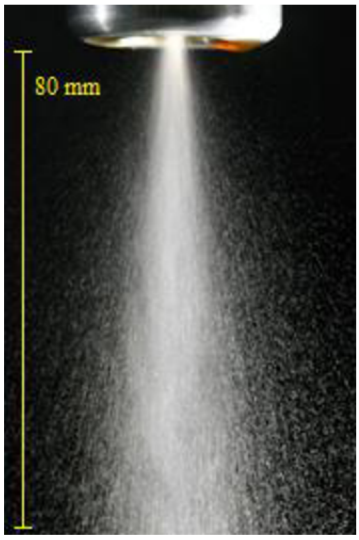

a) GLR=2%, p=2bar

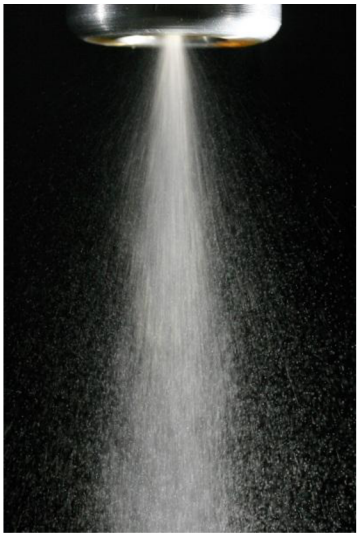

b) GLR=5%, p=2bar

c) GLR=10%, p=2bar

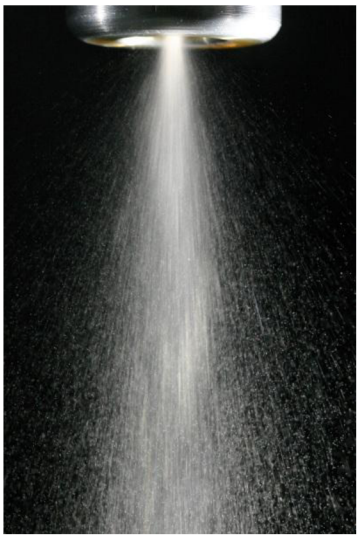

d) GLR=2%, p=3bar

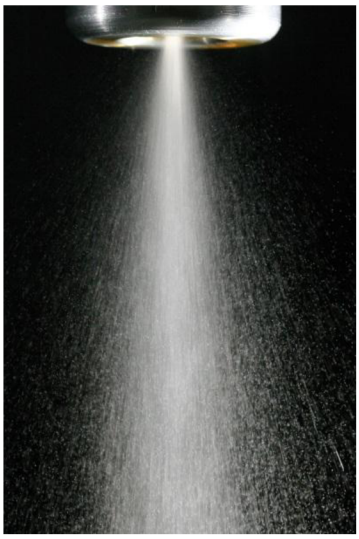

e) GLR=5%, p=3bar

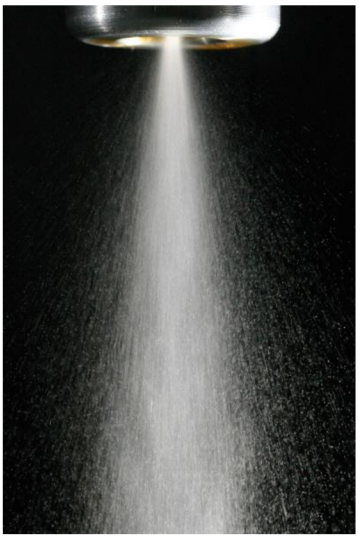

f) GLR=10%, p=3bar

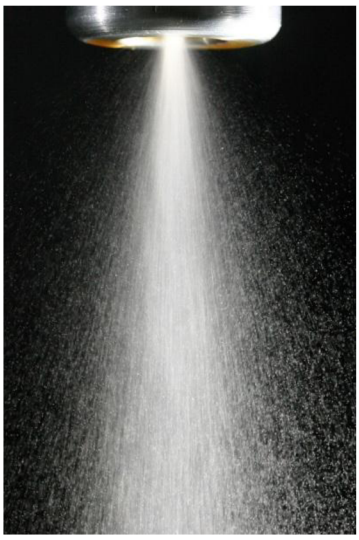

g) GLR=2%, p=4bar

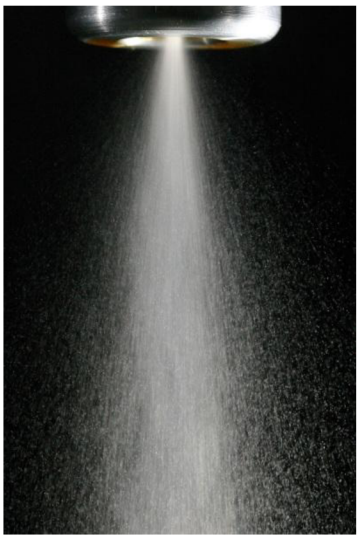

h) GLR=5%, p=4bar

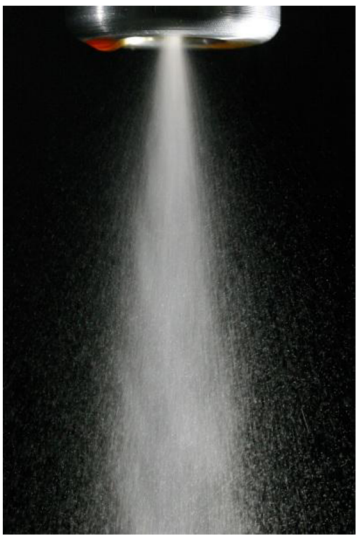

i) GLR=10%, p=4bar

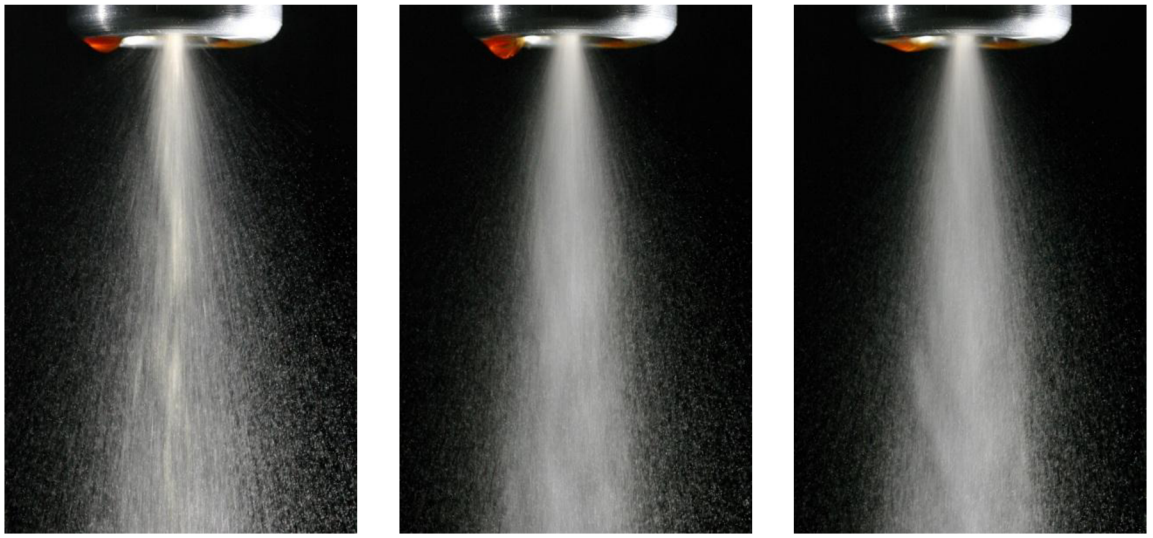

j) GLR=2%, p=5bar k) GLR=5%, p=5bar l) GLR=10%, p=5bar

Figure 7-2 Photos of different flow regimes.

From visual point of view it is obvious that increase in GLR leads to finer atomization and higher velocities of particles in the center of spray. This is due to kinetic energy of atomizing air which accelerates particles during expansion of air (Primary atomization). In photos we can see non-homogenous flows (Figure **7-2** d, j, l). They are caused by pulsation in the nozzle. For detailed distinction high frequency camera was used. From recordings (they are accessible on attached DVD) it is obvious that spray is unstable and high instabilities occur in every flow regime. The following eight frames show the evolution of the pulsation:

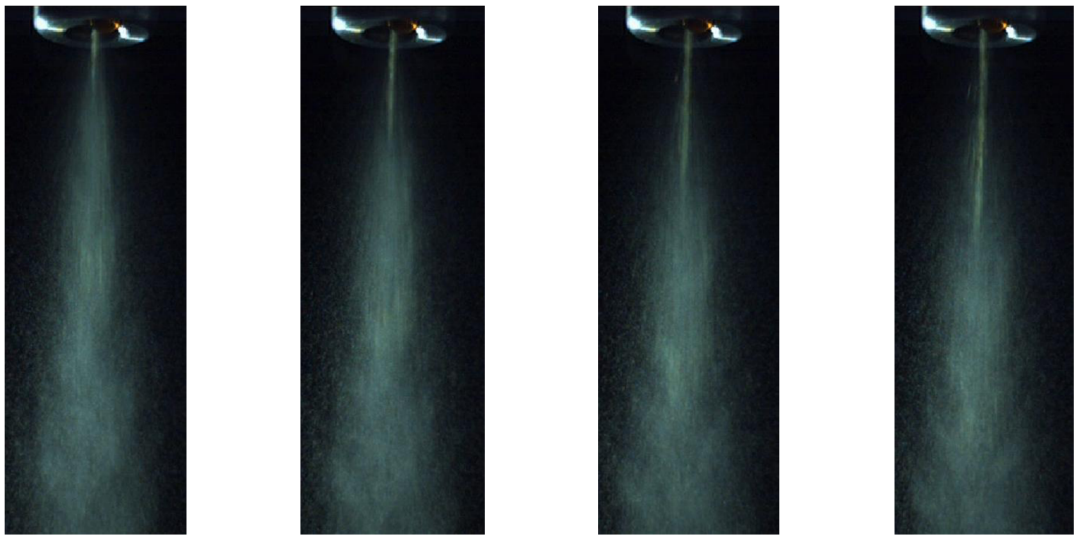

a) b) c) d)

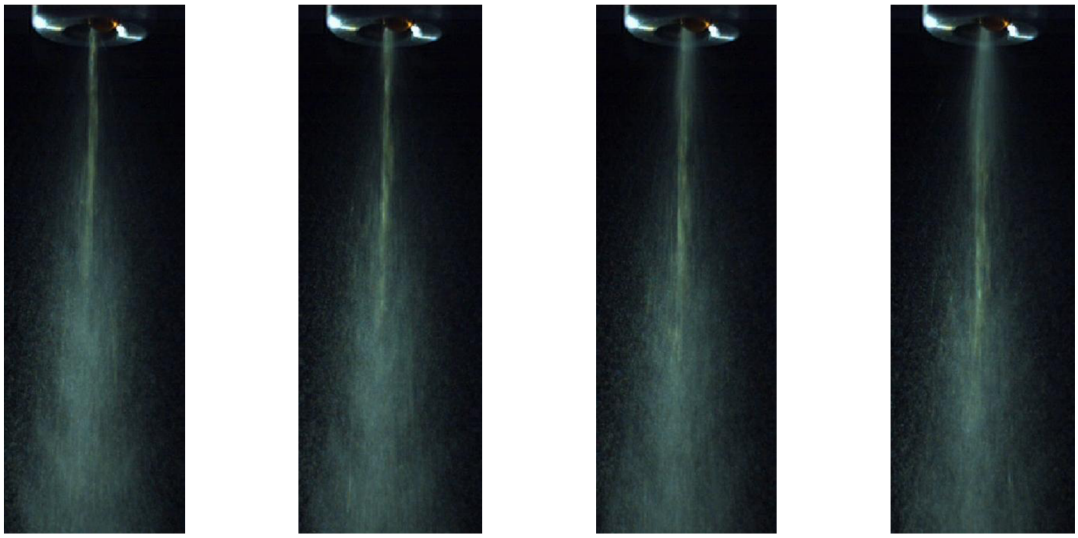

e) f) g) h)

Figure 7-3 Instability in spray (GLR = 2%, p = 2bar).

In the Figure **7-3** it is shown one pulsation which was created by local decreasing in GLR in exit orifice. This leads to fuel flow only and after some amount of fuel passes through orifice the pressured air follows and accelerates surrounding liquid by rapid expansion into ambient air. It acts as some unsteady form of Slug flow.

To examine source of these instabilities the Piezo pressure sensor was mounted into fuel and air loop. The signal was processed by Oscilloscope.

In air loop there was no significant pulsation. It seemed to be relatively stable. Problematic pulsations were measured in fuel loop. There was region of low frequency pulsation (under 100 Hz) and more weaker peaks of high frequency pulsation. The influence of the pump was examined using different settings (using regulation valves and bypass and pump power input) and no relationship was found between RPM (Revolutions per minute) of the pump and frequency of pulsations. This pulsation does not have any specific frequency. They occur almost randomly.

Internal geometry of the aerator was also examined. The number of aerator holes was changed by closing some of the aerator holes. It also does not have any positive influence on the nozzle performance.

The source of the instabilities is attributed to the internal unsteady character of flow and it is of interest for detailed description for future research.

7.1 Cone angle

Cone angle θ is derived from Data rate across the profile in radial direction.

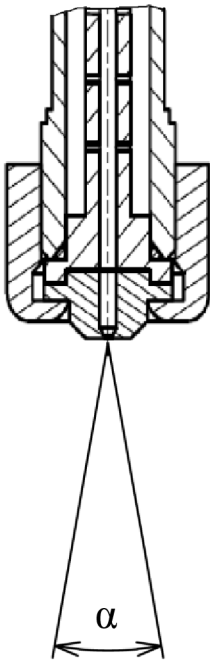

Figure 7-4 Spray Cone angle.

The data rate is counted as mean magnitude from negative and positive direction from the center of the spray. The criterion which determines the cone angle is border of 5 % of Data rate in radial direction. This criterion was chosen as objective measure, which determines edge of spray for each regime using number of samples per second (corresponds to numbers of drops in time). The value was read from graph as the following Figure shows:

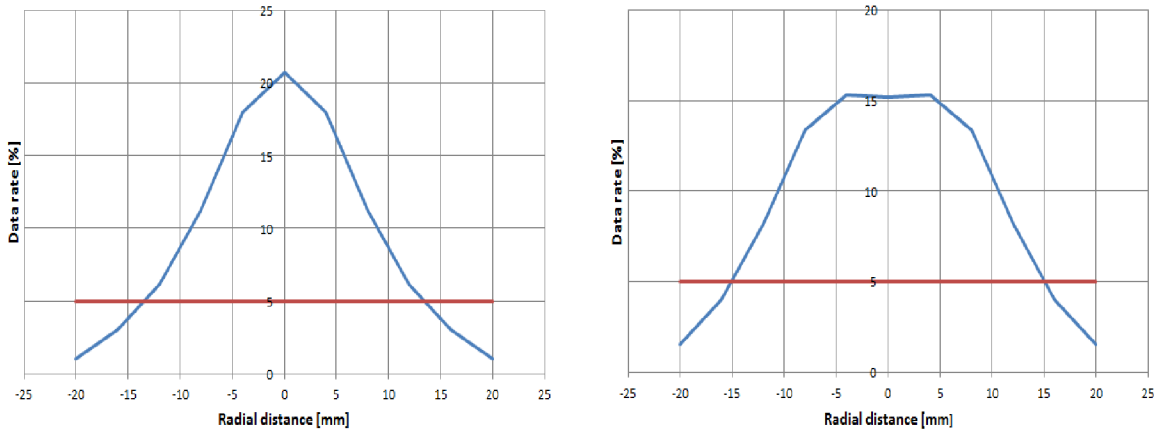

a) b)

Figure 7-5 Data rate distribution for 3bar: a) GLR = 2 %, b) GLR = 10 %.

The red line shows the criterion of 5 % from the Data rate distribution. In the graphs we can see that Data rate profile is flattened as GLR increases. The Data rate distribution corresponds to the axial velocity distribution.

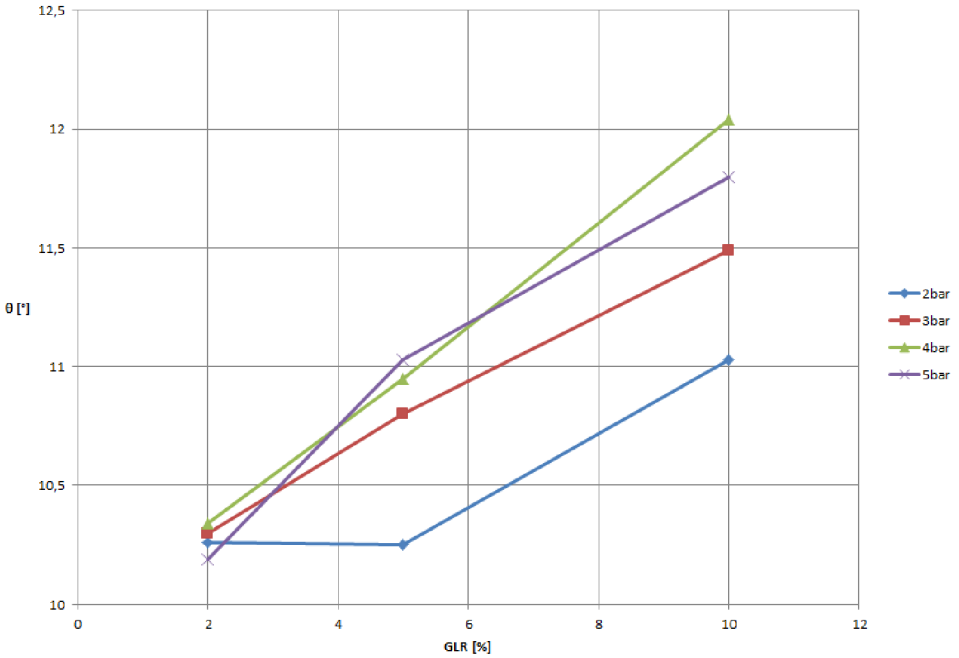

Figure 7-6 Cone angle at 21°C.

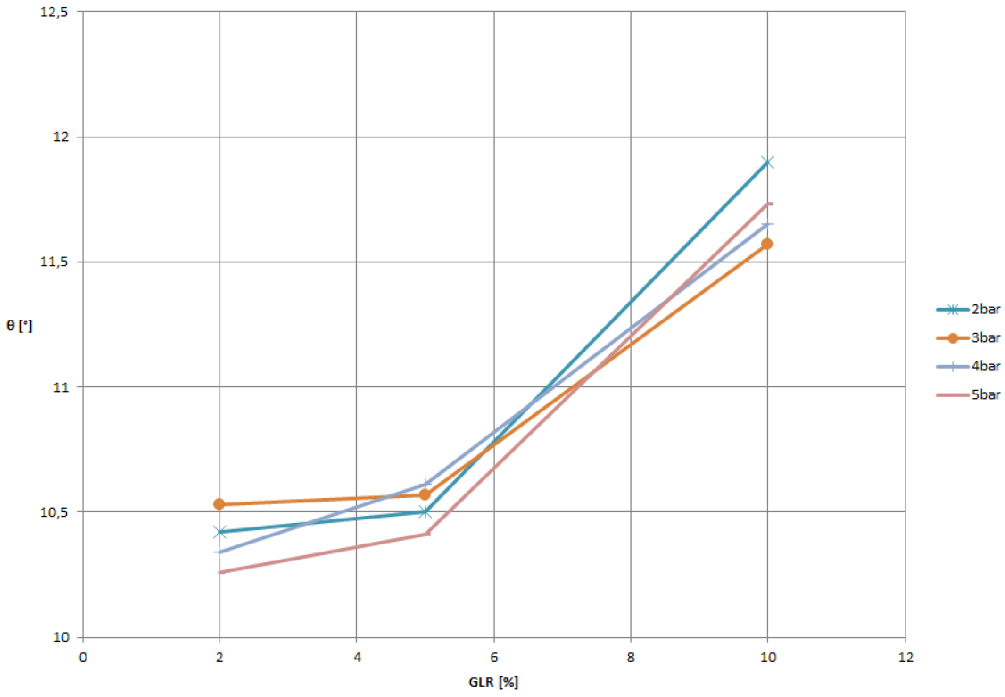

Figure 7-7 Cone angle at 15°C.

The values of Data rate are averaged from two points, which have the same radial distance from the center. This calculation takes into account influence of the optical

access to the measuring volume. In points which are located further from the Receiver the reflected light needs to pass through spray. This increases noise and thus the Data rate decreases compared to the points, which are on the other side of the spray.
Generally, it can be seen that with increasing pressure or GLR the cone angle widenes. This conclusion corresponds to findings of Sovani et al. [5] They attribute this behavior to magnification of energy available for expansion of the air core which tends to spread liquid wider. On the other hand, increase in kinematic viscosity does not show specific relationship with cone angle as it is evident from the **Figure 7-6** Cone angle at 21°C. and

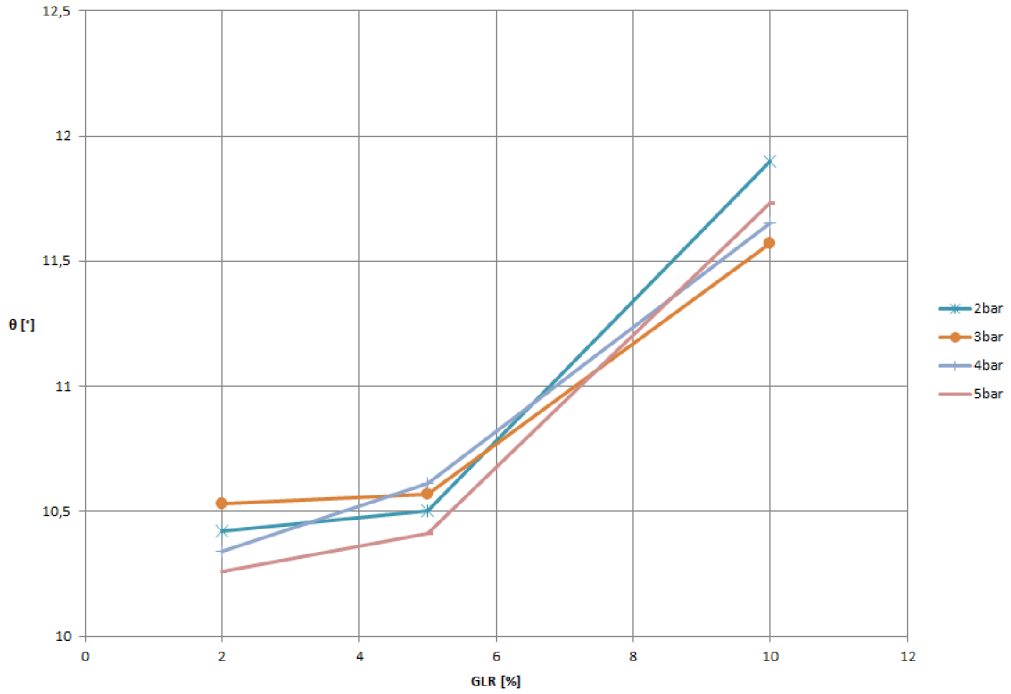

Figure 7-7 Cone angle at 15°C.. Chen and Lefebvre (cited in [5]) pointed out that cone angle increases as liquid viscosity decreases. This conclusion was obtained for Water and Water-corn syrup which might be the reason that our measurements do not conform. From our results the cone angle increases only in 5 % GLR regime except 2 bar regime. Other regimes of GLR conform that more viscous liquid produces generally wider cone angle. To determine characteristic relationship between viscosity and cone angle more experiments are required. For example experiments at more different temperatures.

7.2 Axial velocity profiles comparison

Measurements were performed at z = 150 mm downstream from the nozzle orifice. At this point the spray is fully developed as it is mentioned in [6]. Positions in radial direction were set due to spray width. 11 radial positions were measured with 4 mm space between positions.
Our focus was to compare axial velocities in radial direction in different sprays GLR, pressure and temperature of the atomizing fluid (LHO).
The results are shown in the following graphs:

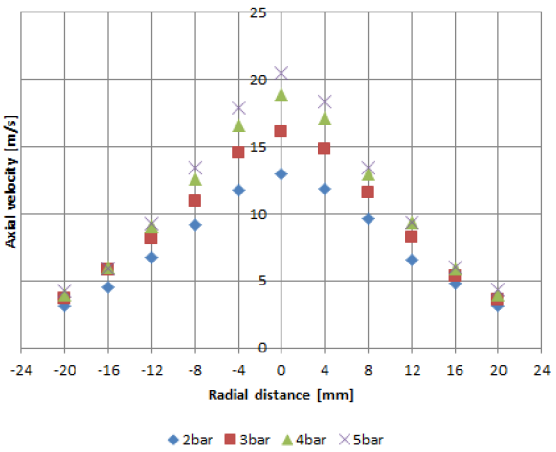

a) Axial velocity at 21°C, GLR=2%

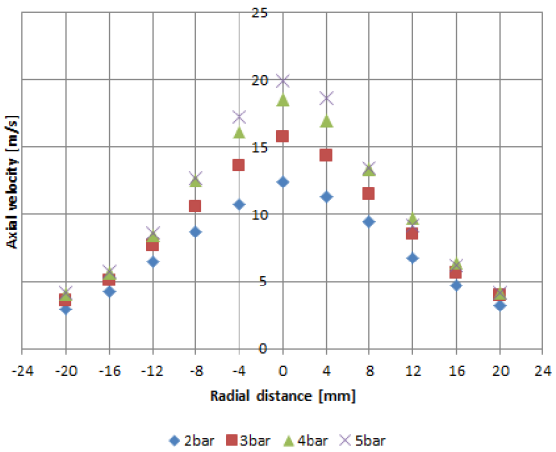

b) Axial velocity at 15°C, GLR=2%

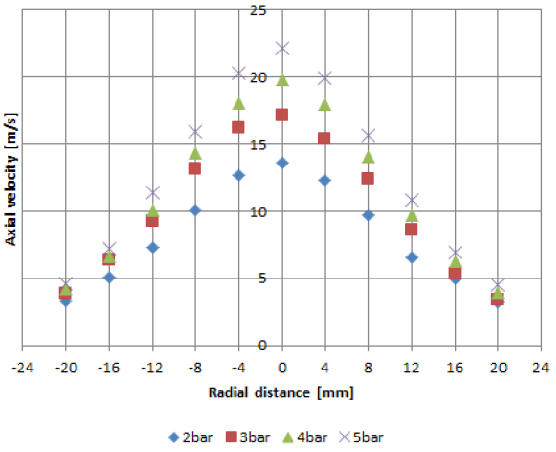

c) Axial velocity at 21°C, GLR=5%

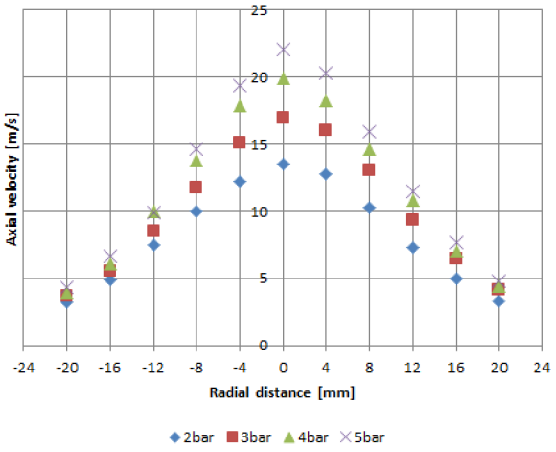

d) Axial velocity at 15°C, GLR=5%

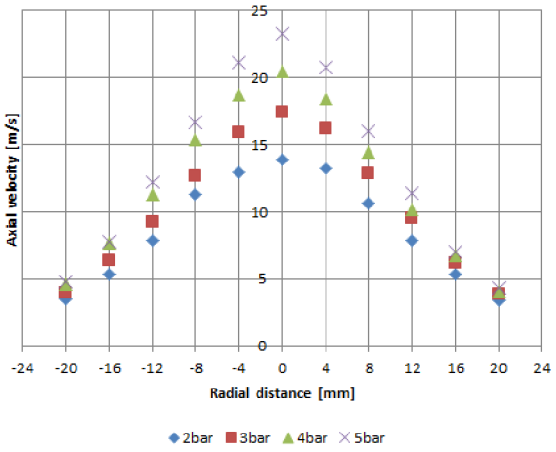

e) Axial velocity at 21°C, GLR=10%

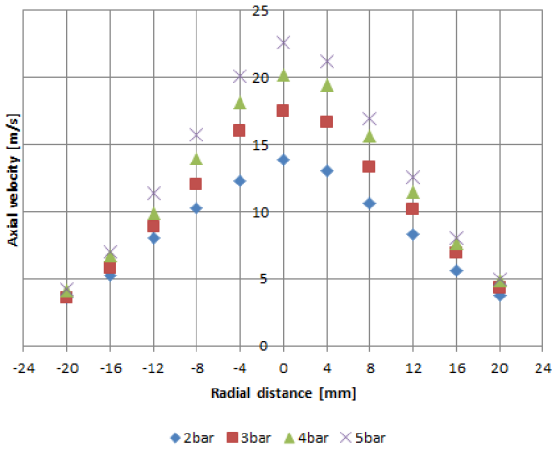

f) Axial velocity at 15°C, GLR=10%

Figure 7-8 Comparison of axial velocity.

The results show that increase in pressure causes higher axial velocities which is consistent with results published by Panchagnula and Sojka cited in [5]. The maximum velocity is in the center of the spray and falls rapidly with radial distance from the center. Viscosity has only small effect on axial velocity distribution. Velocities at 15°C are slightly lower than in normal room temperature (21°C). The biggest difference can be

seen at GLR = 2 %. This behavior can be attributed to the fact that in regime of low GLR there is more fuel, which is not influenced by air temperature, than in regimes with higher values of GLR.
The influence of the axial position of measured profile was examined at six various distances from exit orifice. All measurements were performed at pressure 3 bar and 5 % GLR.

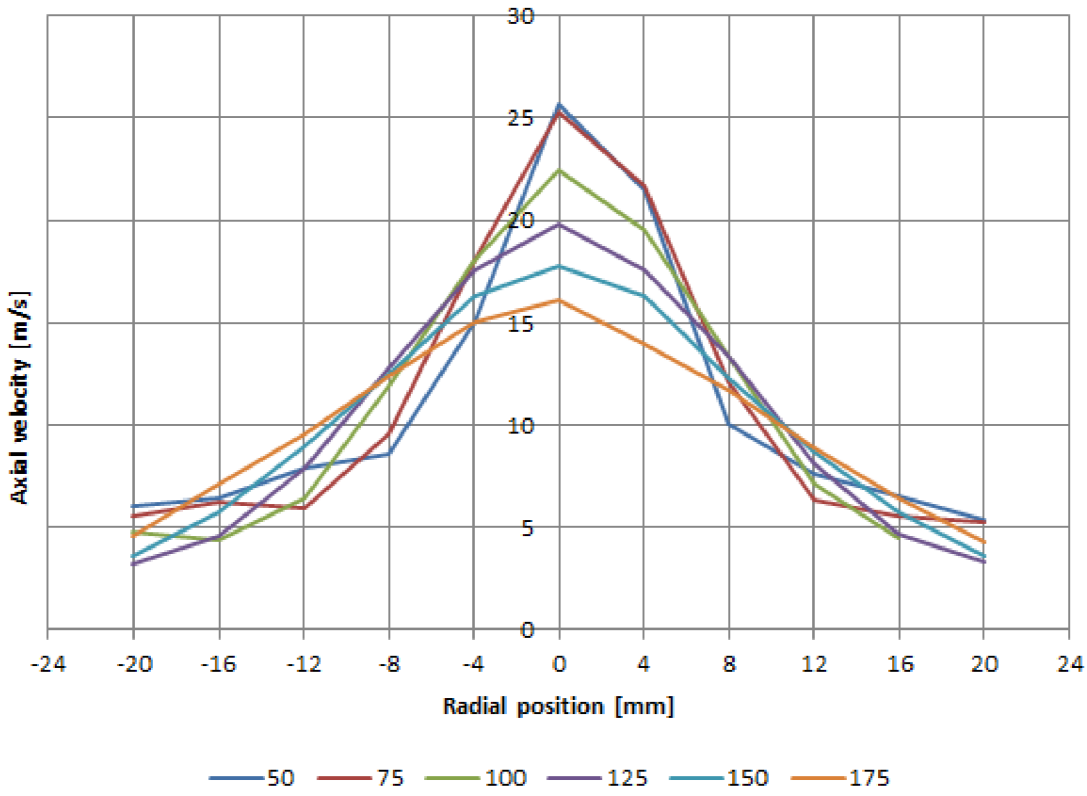

Figure 7-9 Comparison of axial distance and axial velocity.

The axial velocity is highly dependent on axial distance from nozzle. A series of measurements from Sojka [5] are associated with these results. All studies show that axial drop velocity decreases as axial distance from the nozzle increases. Velocity profile becomes also more flattened due to air drag forces. These forces drive droplets to slow down.

7.3 Radial velocity profiles comparison

Radial velocity in sprays indicates fluctuations in sprays. From all measurements it can be seen that the lowest value of the radial velocity is in the center ≈ 0 m/s. This means that in the center the axial velocity is dominant. Radial velocity has maximum at 12 mm from the center for each flow regime. Maximum value changes with initial pressure and GLR. Increase in GLR leads to increasing radial velocity maximum value. For most regimes the higher pressure leads to higher radial velocities. But it should be pointed out that, in regime of GLR = 2 % the maximum pressure does not match to the highest value of the fluctuation velocity. The highest radial velocity is at 3 bar for 21°C and at 4 bar for 15°C. The measurements at 15°C have higher maximum value of radial velocity.
Generally, the radial velocity determines the rate of fluctuations. The results show that fluctuations are biggest around 12 mm from the center of the spray. This is the area where droplets have high axial speed but are all dragging due to air drag forces.

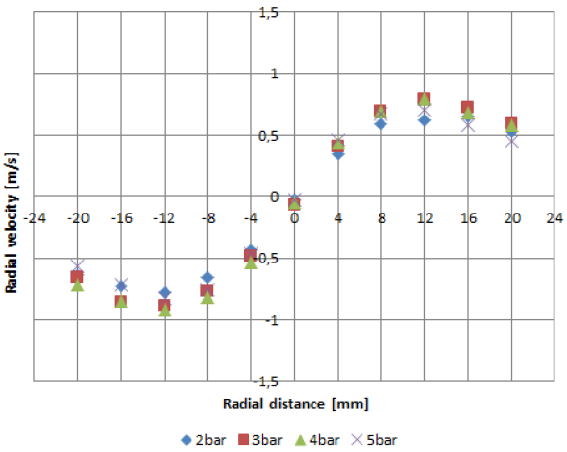

a) Radial velocity at 21°C, GLR=2%

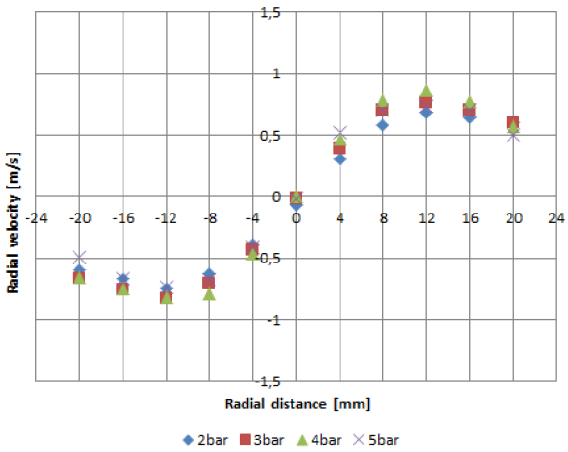

b) Radial velocity at 15°C, GLR=2%

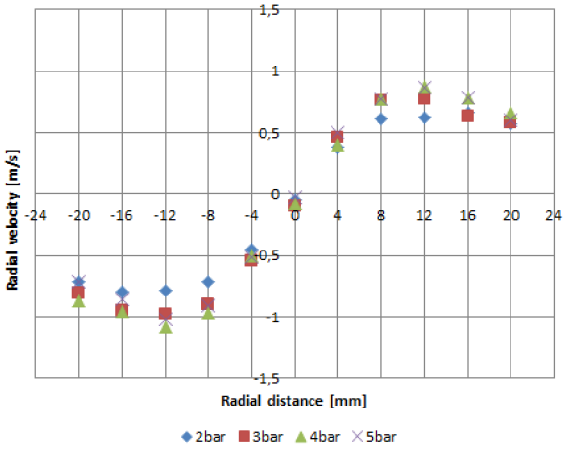

c) Radial velocity at 21°C, GLR=5%

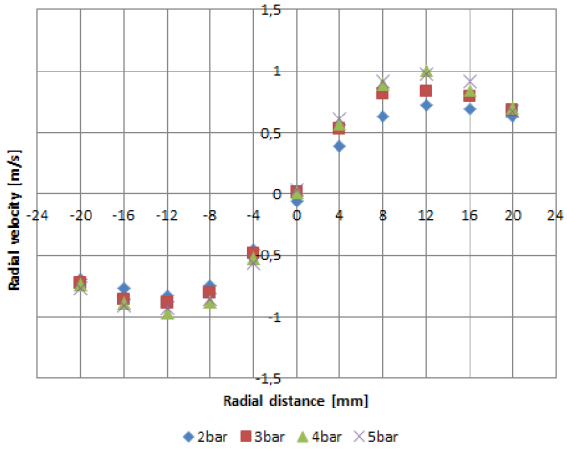

d) Radial velocity at 15°C, GLR=5%

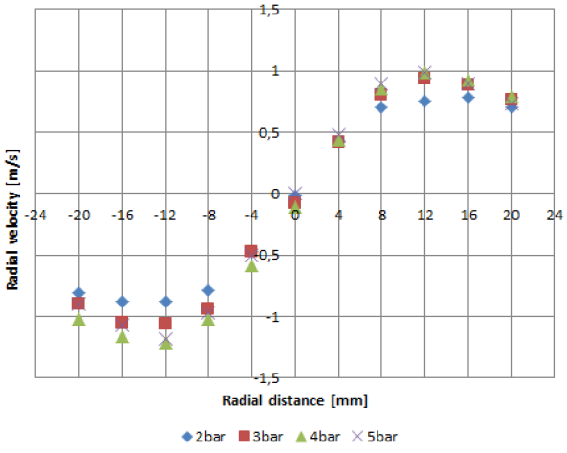

e) Radial velocity at 21°C, GLR=10%

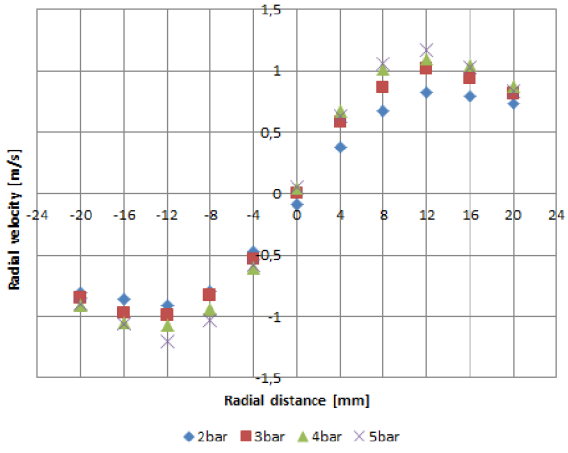

f) Radial velocity at 15°C, GLR=10%

Figure 7-10 Comparison of radial velocity.

Axial position of measured profile was examined in six different distances from nozzle. Following Figure shows radial velocity profiles.

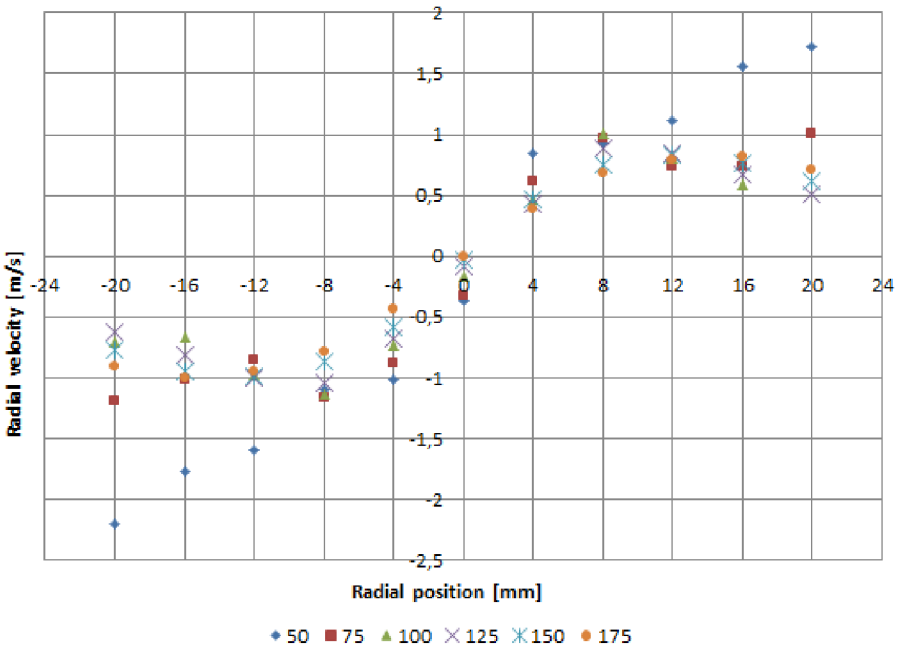

Figure 7-11 Dependency of radial velocity on axial distance from nozzle.

Results show that radial velocity decreases as distance from the nozzle increases. Drag forces are dependent on the square of particles velocity thus the biggest difference can be seen between 50 and 75 mm where are also the fastest particles (as we can see in the Figure **7-11**).

7.4 Drop size distribution

Drop size is one of the most important parameters of the spray. For consistent description the SMD diameter is used for most applications for combustion processes. Following Figures show dependency of SMD on pressure and GLR:

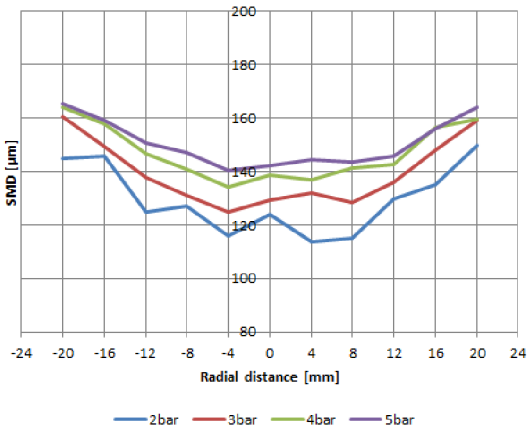

a) SMD distribution at 21°C, GLR =2%

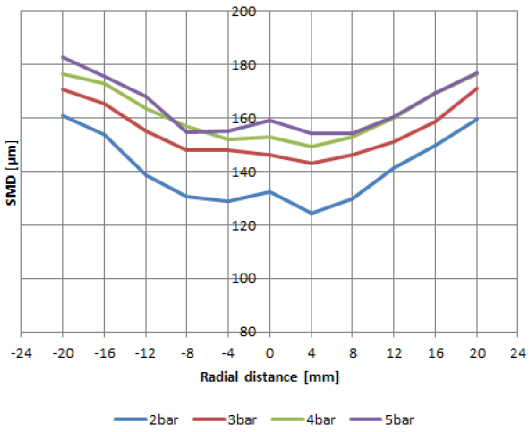

b) SMD distribution at 15°C, GLR =2%

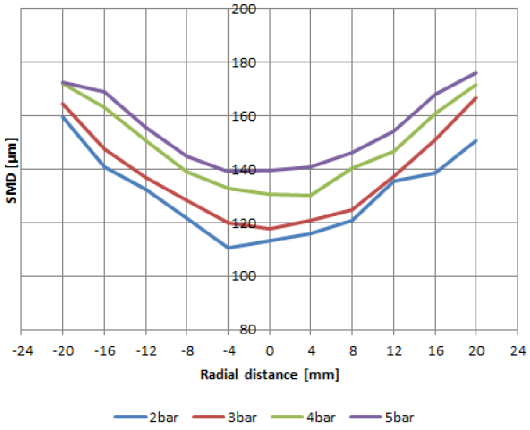

c) SMD distribution at 21°C, GLR =5%

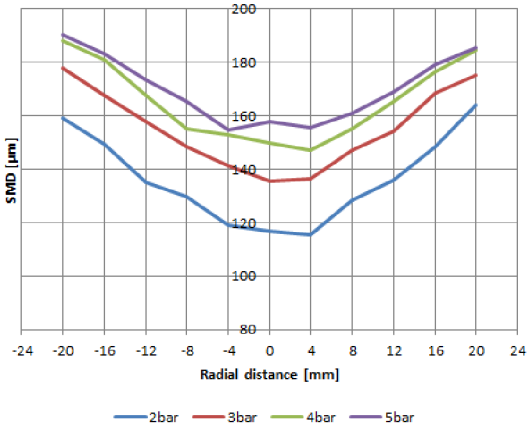

d) SMD distribution at 15°C, GLR =5%

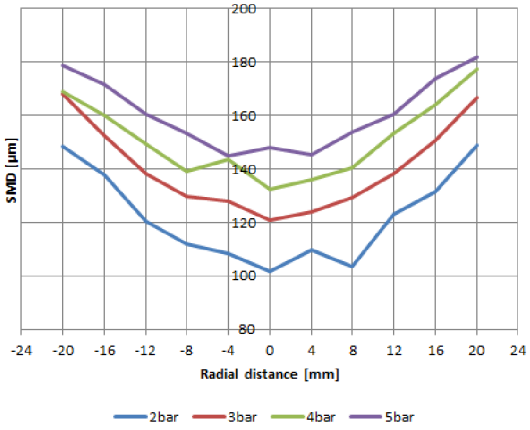

e) SMD distribution at 21°C, GLR =10%

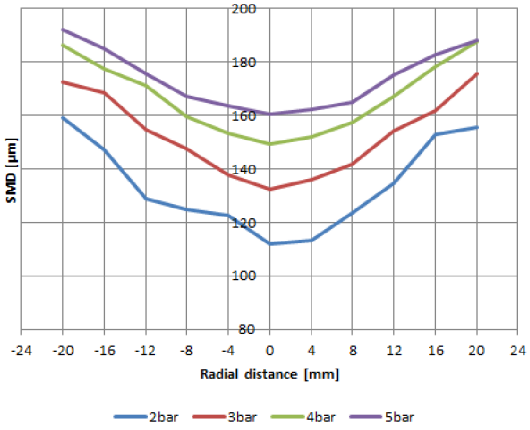

f) SMD distribution at 15°C, GLR =10%

Figure 7-12

As was mentioned in [5] and [6] the droplets size decreases when GLR increases. This behavior is attributed to the influence of the amount of atomizing air which inclines liquid to break up intensely. It corresponds to findings mentioned in Chapter 2. The shape of SMD profile changes also with GLR. The increase of GLR leads to flatter minimum positioned in the center of the spray.

On the other hand, the influence of the pressure has significantly different behavior than was expected. The results show that increase in the initial pressure leads to bigger droplets. This behavior was attributed to the instabilities mentioned at the beginning of this chapter. The records from high frequency camera prove this statement. It can be seen that higher pressure leads to higher frequency of instabilities and thus to greater amount of large droplets which has significant influence on the SMD value. The influence on the D_{10} is smaller, because it is not dependent on droplet volume but on the droplet diameter. D_{10} measurements indicate the same result as SMD.
Next graphs show dependency of weighed SMD on initial pressure and GLR at two different temperatures. Weighted SMD takes into account a Data rate in each measured point.

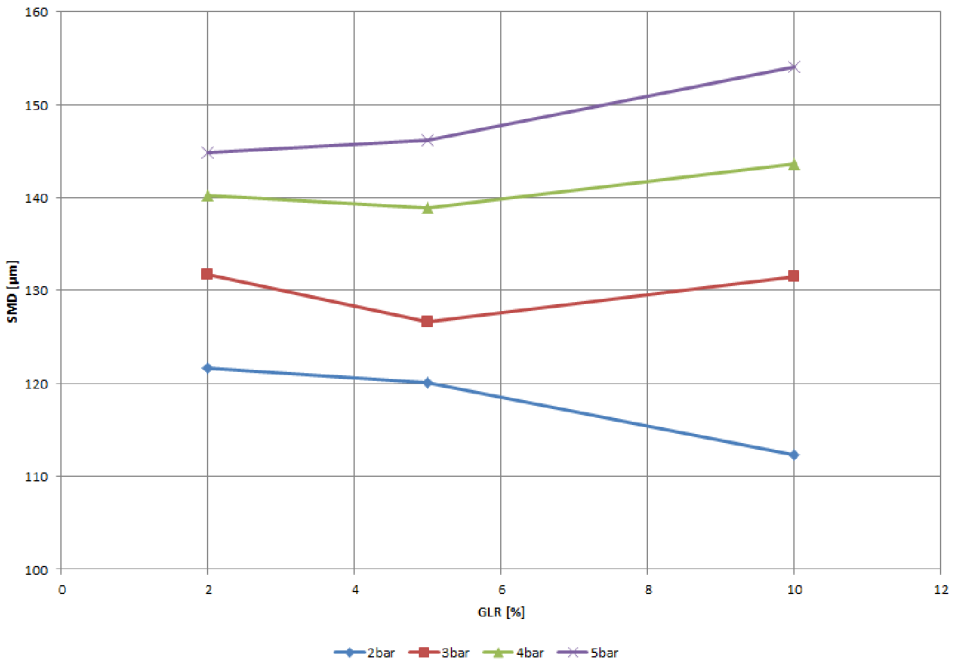

Figure 7-13 Weighted SMD at 21°C.

These graphs show that SMD increases as pressure increases. Odd behavior can be seen with increasing GLR. Due to findings cited in [5], [6] the SMD decreases with increasing GLR, but in our case it is valid only for low pressures. The point to note here is that the pulsation described above might have influence on this behavior. As GLR increases the frequency of pulsations increase and produce more large droplets which influence the SMD. The next reason for this result might be that PDA measures the large droplets, which reflect stronger signal even passing the edge of measuring volume and drown out the weaker signal from small particles.
Results from measurement at 15°C show that increase in kinematic viscosity leads to larger droplets. Viscosity prevents atomizing liquid to break up. To achieve the same SMD at lower temperature, higher initial pressure or GLR is needed. Satapalthy et al. cited in [5] obtained similar findings. They pointed out that mean drop size is strongly dependent on liquid viscosity and increases markedly with an increase in viscosity.

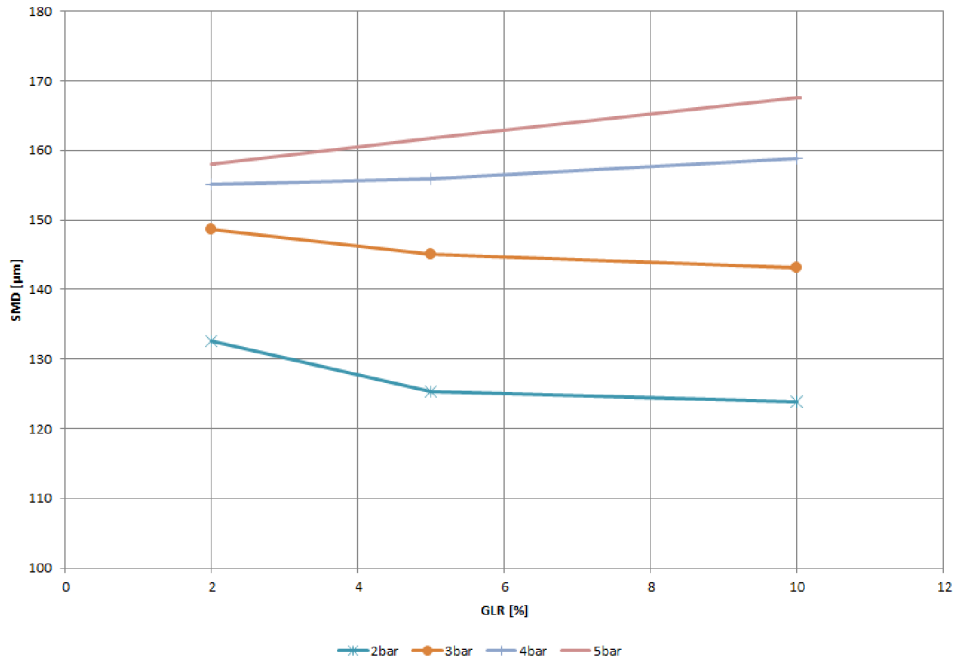

Figure 7-14 Weighted SMD at 15°C.

The influence of axial distance from nozzle was examined in six positions. Measurements show that SMD increases with increasing axial distance from nozzle.

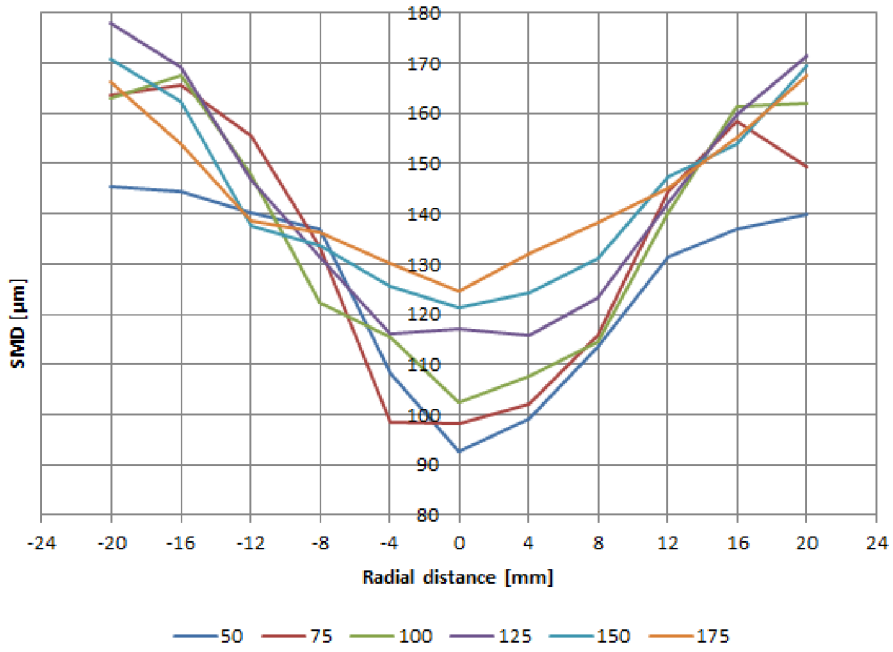

Figure 7-15 Comparison of axial profiles on SMD distribution.

This result corresponds to the findings by Withlow and Lefebvre cited in [5] for regimes with higher GLR (> 1 %). This behavior was attributed to combined effects of drop coalescence.

7.5 Measurement uncertainty

[11]

The confidence limits for the Mean and RMS values are 95%. They are computed online during acquisition respecting following equations:

Mean: $$1.96 \times \sqrt{\frac{\overline{U^2}}{N}}. \quad (7.1)$$

RMS: $$1.96 \times \sqrt{\frac{\overline{U^2}}{2N}}. \quad (7.2)$$

It is also required that samples need to be independent. Otherwise, N must be replaced by the effective number of samples irrespective of the number of samples actually taken:

$$N_{eff} = \begin{matrix} \frac{T_m}{2\tau_l} & if\ N > \frac{T_m}{2\tau_l} \\ N & \text{otherwise} \end{matrix} \quad (7.1)$$

Where Tm is the time between first and last sample. The τ_l is the integral time scale of the flow, which must be estimated either by hand or based on the samples themselves.

8. CONCLUSION

This chapter generally concludes the whole thesis. In the first paragraph is goals, which have been achieved, are summarized. The second part evaluates results from measurements.

8.1 Goals

The goals were mentioned in preface of this work. They were:

- Production documentation of jets (Chapter 3)
- Experimental setup of testing rig (Chapter 5)
- Preparation and setup of optical measuring system (Chapter 6)
- Measurement of spray characteristic (Chapter 7)
- Analysis of results and their graphical presentation (Chapter 7)

Point two and three took more time than was excepted due to problems with laser argon tube and laser power supply system. They had to be sent to the complaint. That is why the work had a few months delay. But in the end everything was managed in time.
The PDA systems is now functional and continously monitored for following experiments. Author of this thesis participated two workshops about laser techniques from Dantec and Dr. Graham Wigley. Thanks to this experience was able to prepare whole measurement.

8.2 Spray characteristics

This section deals with the Effervescent atomizer which was designed especially for this application. The data was obtained by PDA measuring system which enables to measure droplet velocity and droplet size.
PDA system was assembled and optimized for given application. It is a large and complicated system and its condition should be monitored over time.

Measurements show that velocity distribution has similar results as was excepted. Velocity increases with the pressure and GLR. Droplet size distribution varies with pressure and GLR. Experiments show that drop size is highly dependent on GLR. Increase in GLR leads to a decrease in droplet size. But increase in pressure does not correspond to decrease in particles diameter. It has resulted in opposite behavior than was excepted. As pressure increases the droplet diameter also increases. This result was attributed to pulsations which were examined by photos and recordings from high frequency camera. Experiment with Piezo pressure sensor in fuel loop does not show any relationship between pulsations and pump RPM. That is why pulsation was attributed to the internal dynamic flow behavior and it is of importance for further research. Another

un-excepted behavior was in weighted values of SMD. These results were attributed to pulsations which might have influence on PDA measurement.

Due to time pressure the influence of the internal geometry of atomizers has not been examined and it is of interest for future research. Also optimizing the test bench could lead to improvements in jet performance. To achieve non-pulsating flow in fuel loop the pump might be resolved using pressure tank instead of pump or mounting a dynamic dumper into loop.

The developments of Effervescent atomizers were mostly experimental. At this moment it is not possible to analytically describe effervescent performance. The results of this thesis show that this type of atomizers does not behave exactly as previous researchers reported and for detailed description of this issue more experiments are required.

Bibliography

[1] Lefebvre, A., Ballal, D. R. *Gas Turbine Combustion*. CRC Press, 3rd edition, 2010. 560 p. ISBN 978-1-4200-8605-8.

[2] Lefebvre, A.H., *Atomization and Sprays*, Hemisphere, Washington, D.C., 1989

[3] Ďurdina L, *MEASUREMENT OF SPRAY CHARACTERISTICS USING OPTICAL MEASUREMENT METHODS*, VUT Brno, 2012

[4] http://www.thermopedia.com, 2013-3-12

[5] Sovani S.D. et al., *Effervescent atomization* Laboratories (formerly Thermal Sciences and Propulsion Center), School of Mechanical Engineering, Purdue University, West Lafayette, IN 47907-1003, USA Cran®eld Institute of Technology, and Purdue University, West Lafayette, IN 47907-1003, USA, Received 5 May 1999; accepted 5 November 2000

[6] Jedelsky J. et al., *Development of an Effervescent Atomizer for Industrial Burners*, Faculty of Mechanical Engineering, Brno University of Technology, Received June 30, 2009. Revised Manuscript Received October 14, 2009

[7] Bayel, L., Orzechowski, Z., *Liguid atomization*, Taylor & Francis, Washington, D.C., 1993

[8] Liu, H. *Science and Engineering of Droplets*. Noyes Publications, 2000. 534 p. ISBN 0-8155-1436-0

[9] Lin S.P., *Breakup of Liquid Sheets and Jets*, CAMBRIGE UNIVERSITY PRESS 2003

[10] Pavelek M., Janotková E., Štětina J.: *Vizualizační a optické měřicí metody*, Accessed via WWW, URL: http://dt.fme.vutbr.cz/~pavelek/optika/, (31 Oct. 2006).

[11] *LDA and PDA Reference Manual by Dantec*, 1st edition, 2011

[12] Dantec Dynamics, *PDA slideshow*, [2011?] available from: http://www.dantecdynamics.com/Default.aspx?ID=455

[13] Wigley G, *INTRODUCTION TO LIGHT SCATTERING AND OPTICAL DIAGNOSTICS FOR THE ANALYSIS LIQUID SPRAYS*, Department of Aeronautical and Automotive Engineering, Loughborough University, [2010?]

[14] Coriolis flowmeters Sitrans F C MASS 2100 Di 3-40. Siemens, July 2010. Available from: http://cache.automation.siemens.com/dnl/jg/jgxNzQ2MwAA_45027364_HB/MASS2100_3-40_OI_En_en-US.pdf

[15] http://www.omega.com/Manuals/manualpdf/M2842.pdf, 2013-3-12

[16] *Omega, SPRTX and STCTX Series reference manual*, Information available: http://www.omega.com/Temperature/pdf/SPRTX_STCTX.pdf, 2013-3-12

[17] Information avaible from: http://www.bdsensors.cz/fileadmin/user_upload/Download/Datenblaetter_datasheets/DMPi-LMPi_CS.pdf

[18] Lin S.P., *Breakup of Liquid Sheets and Jets*, CAMBRIGE UNIVERSITY PRESS 2003

[19] Stabilite 2017 User's Manual Spectra Physics, Part Number 0000-215A, Rev. D, June 2001

[20] H. Summers: Theory of viscosity measurement, Accessed via WWW. http://www.hanssummers.com/electronics/viscometer/theory.htm (19 Sept. 2006).

List of symbols

Roman symbols

A	surface area, m^2
A_1	experimental constant in viscosity calculation
A_0	orifice area, m^2
A_h	area of the aerator holes, m^2
D	droplet diameter, m,
d	inner diameter of the aerator, m
$D_{0.1}$	drop diameter such that 10 percent of total liquid volume is in drops of smaller diameter, m
$D_{0.5}$	median drop diameter, m
$D_{0.632}$	characteristic diameter; 63.2 percent of total liquid volume is in drops of smaller diameter, m
$D_{0.9}$	drop diameter such that 90 percent of total liquid volume is in drops of smaller diameter, m
D_{10}	arithmetic mean diameter, m
D_{20}	surface area mean diameter, m
D_{21}	mean diameter (surface area / length), m
D_{32}	Sauter mean diameter (volume/surface), m
D_{43}	Herdan mean diameter, m
dx	height of measuring volume, m
dy	width of measuring volume, m
dz	length of measuring volume, m
E	energy, J
Ev	experimental constant in viscosity calculation
f_D	Doppler frequency, Hz
f_0	Bragg cell frequency, Hz
k	Boltzmann's constant
l	length of aerator, m
m	mass, kg
N	number of samples
N_f	number of fringes
N_{eff}	effective number of samples
Q	volume, m^3
q	measure of droplet spread in the Rosin-Rammler equation,
Tm	time between the first and the last sample, s
u_x	droplet velocity in x-axis direction, $m \cdot s^{-1}$
We	Weber number
X	constant in Rosin-Ramler distribution
z	distance from nozzle in z-axis direction

Greek symbols

α	mean volumetric expansion,
β_i	geometrical factor
δ_f	distance between fringes, m
θ	cone angle, rad
λ	wavelength, m
μ	dynamic viscosity, Pa·s
ν	kinematic viscosity, $m^2 \cdot s^{-1}$
ρ	density, $kg \cdot m^{-3}$
σ	surface tension, $N \cdot m^{-1}$
τ	shear stress, Pa
τ_I	integral time scale
Φ	phase difference,
ϑ_i	scattering angle, rad
φ_i	scattering angle, rad
ψ_i	scattering angle, rad

Abbreviations

GLR	gas to liquid ratio, %
LDA	Laser Doppler Anemometry
LHO	Light Leating Oil
PDA	Phase Doppler Anemometry
RMS	Root Mean Square
RPM	revolutions per minute, min^{-1}
SMD	Sauter mean diameter (volume/surface), m
SNR	signal to noise ratio

Subscripts

0	initial condition
D	related to Doppler frequency
f	related to frequency
h	related to aerator holes
L	related to liquid
o	related to orifice

List of attachments

Drawings

- Assembled jet (format A1)
- Body (format A3)
- Nozzle (format A4)
- Reduction part (format A4)
- Universal matrix (format A4)
- Long aerator (format A4)
- Short aerator (format A4)

DVD contents

The DVD attached to the thesis contains:

- thesis document in PDF format
- drawings of manufactured jet in PDF format
- photos of examined spray
- recordings from high frequency camera
- program for data acquisition